Electrophysiological investigations of the anterior and posterior lateral line nerve of the Goldfish, *Carassius auratus*, to running water and oscillatory stimuli

Dissertation

Boris Philippe Chagnaud
Weingarten

Bonn 2006

Angefertigt mit Genehmigung der Mathematisch-Naturwissenschaftlichen Fakultät
der Rheinischen Friedrich-Wilhelms-Universität Bonn

1.Gutachter: Prof. Dr. Horst Bleckmann
2.Gutachter: PD Dr. Joachim Mogdans

Tag der mündlichen Prüfung: 13.12.2006

Diese Dissertation ist auf dem Hochschulschriftenserver der ULB Bonn
http://hss.ulb.uni-bonn.de/diss_online elektronisch publiziert

Erscheinungsjahr: 2007

Acknowledgements:

I would like to thank Prof. Horst Bleckmann for the opportunity to work in his lab and for his support. PD Michael Hofmann suggested analysis methods in all parts of this work and deserves my gratitude for numerous contributions in computing macros for data analysis. PD Joachim Mogdans always was very helpful while facing technical and analytical problems.
Martin Müller helped with the graphics and Michel Bauer was involved in the discussion that lead to the idea for the double recordings.

Horst Bleckmann, Joachim Mogdans and Michael Hofmann helped improved considerably the manuscript and were involved in countless fruitful discussions.

Parts of this work have been submitted for publication:

I) Journal of comparative physiology A

II) Journal of zoology

III) Journal of comparative physiology A

Abstract

The neural responses of anterior lateral line nerve (ALLN) fibers of goldfish to sinusoidal water motions in still and running water were investigated. In agreement with previous data (Engelmann et al., 2002) two types of fibers were distinguished: type I fibers, which most likely innervate superficial neuromasts, were stimulated by running water (10 $cm*s^{-1}$) and, type II fibers, which most likely innervate canal neuromasts, were not stimulated by running water. The responses of type I fibers to sinusoidal water motions were masked in running water whereas responses of type II fibers were not masked. The degree of response masking increased with increasing flow velocity. Moreover, the ratio between responses that were masked in running water (type I) and those that were not masked (type II) increased with increasing flow velocity. Fibers exposed to unidirectional water flow showed a continuum of flow sensitivity and not two separate populations of flow sensitive and flow insensitive fibers as might be expected from previous results and theoretical considerations. Most nerve fibers responded with an increase in discharge rate, irrespective of flow direction (head-to-tail and tail-to-head flow). Thus fibers showed no directional sensitivity. Frequency spectra of water motions quantified with particle image velocimetry (PIV) and spectra of the firing rate of lateral line fibers showed an increase in amplitude below 10 Hz under flow conditions. This suggests that the neuromasts responded to the flow fluctuations that developed under flow conditions, but not to the d.c. flow. Thus it is unlikely that the spike trains of individual fibers code for the direction and velocity of a constant flow. Spike trains of ALLN fibers stimulated by a Kármán vortex street (KVS) showed that low frequency stimuli can still be encoded under running water. In terms of spike rate there was no difference between the KVS and the running water condition. However, if exposed to vortex stimuli, spike train frequency spectra showed reproducible peaks at the vortex shedding frequency. Any change in the vortex shedding frequency evoked by a change in either cylinder diameter or water flow velocity shifted the reproducible peaks of the neuronal data into the expected direction. Thus the data show that information about the frequency composition of flow fluctuation is preserved in the spike trains under flow conditions despite the fact that the fibers do not code for the direction and velocity of the flow.

Abbreviations

ALLN	anterior lateral line nerve
PLLN	posterior lateral line nerve
SN	superficial neuromast
CN	canal neuromast
SW	still water
RW	running water
PIV	particle image velocimetry
VSF	vortex shedding frequency
KVS	Kármán vortex street
cVSF	calculated vortex shedding frequency
a.c.	alternating current
d.c.	direct current
FFT	fast Fourier transformation
IF	instantaneous frequency
RMS	root mean square
RF	receptive field
n	number of cells
N	number of fishes

Introduction

The lateral line is a sensory system used by fishes and aquatic amphibians to detect minute water motions (Bleckmann, 1994). It can play a dominant role in many behaviors including rheotaxis (Kanter and Coombs, 2003; Montgomery et al., 1997; Simmons et al., 2004), schooling behavior (Partridge and Pitcher, 1980), object recognition (Campenhausen et al., 1981), communication (Satou et al., 1994), prey capture (Kanter and Coombs, 2003; New et al., 2001) and predator avoidance (Blaxter and Fuiman, 1990).

The sensory units of the lateral line are the neuromasts (Northcutt, 1989). In fish, two types of neuromasts are found, superficial neuromasts (SN) located on the skin and, canal neuromasts (CN) situated in sub-dermal fluid-filled canals that are connected to the outside medium by pores (Bleckmann, 1993; Coombs et al., 1988; Münz, 1989; Puzdrowski, 1989). Typically there is one CN between two adjacent canal pores (Disler, 1977; Engelmann et al., 2002; Puzdrowski, 1989; Webb, 1989). Goldfish have up to 200 CNs and up to 3000 SNs distributed over their head, trunk and tail fin (Puzdrowski, 1989). CNs are oriented parallel to the length axis of the respective canal (Engelmann et al., 2002). Most SNs are oriented either parallel or orthogonal to the body axis (Coombs et al., 1988; Engelmann et al., 2002).

Lateral line neuromasts may contain up to several hundred hair cells, each of which carries up to 150 stereovilli and a single true kinocilium at the apical surface. The stereovilli grow longer from one edge of the hair bundle to the other. The kinocilium always occurs eccentrically at the tall edge of the bundle, thus all hair cells have a morphological polarization. The ciliary bundles of the hair cells are embedded in a gelatinous cupula that extends into the surrounding water or into the canal fluid (Flock, 1971; Jørgensen and Flock, 1973). The sensory epithelium of a lateral line neuromast contains two antagonistically orientated populations of hair cells (Flock and Wersäll, 1962).

The hair cells of the neuromasts on the trunk of the fish are innervated by afferent and efferent fibers of the posterior lateral line nerve (PLLN). Neuromasts on the head are innervated by fibers of the dorsal or ventral anterior lateral line nerve (ALLN) (Puzdrowski, 1989). Individual afferent fibers innervate either a single CN or one or several SNs (Münz, 1985). Single lateral line nerve fibers may innervate more than one hair cell, provided they have the same orientation (Görner, 1963).

Lateral line hair cells are displacement detectors. A water induced displacement of the cupula results in a shearing of the hair bundles that leads to a change of the hair cells resting potential. Displacement of the ciliary bundle towards the kinocilium causes a depolarization, displacement in the opposite direction a hyperpolarization of the hair cell (Kroese and van Netten, 1989). Displacement of the cupula leads to an increase in discharge rate of fibers innervating one population of hair cells and to a decrease in discharge rate of fibers innervating the hair cells aligned in the opposite direction. SNs function as velocity detectors, i.e., they respond proportional to the velocity of the water surrounding the cupula. In contrast, CNs function as acceleration detectors, i.e., they respond proportional to the acceleration of the water outside the canal (Kroese and Schellart, 1992). CNs can also be considered as pressure gradient detectors since water flow inside the canals is only generated by pressure differences between canal pores (Coombs et al., 1996; Denton and Gray, 1988). With respect to water velocity, lateral line canals act as high-pass filters (Denton and Gray, 1988). Consequently, CNs should not be stimulated by laminar d.c. water flow (Denton and Gray, 1988; Voigt et al., 2000). CNs should respond, however, to the a.c. components of prey generated water motions even in the presence of d.c. water flow.

When fish are exposed to unidirectional water flow, two types of afferent lateral line fibers can be distinguished, those that respond to increasing flow velocity with increases in discharge rate and those that are insensitive to unidirectional water flow (Carton and Montgomery, 2002; Engelmann et al., 2002; Voigt et al., 2000). There are only incidental reports of fibers that respond to increasing flow velocity with decreases in discharge rate (Carton and Montgomery, 2002; Görner, 1963). In the PLLN of goldfish afferent fibers have been classified as type I and type II

(Engelmann et al., 2000). Type I fibers responded with an increase in discharge rate to a 10 cm*s^{-1} water flow whereas type II fibers were insensitive to that flow. As a consequence, the responses of type I fibers to sinusoidal water motions generated by a vibrating sphere were masked by the flow. In contrast, type II fibers responded about equally well to the vibrating sphere in still and running water. These findings suggested that type I fibers innervate SNs while type II fibers innervate CNs (Engelmann et al., 2002). In this study it was investigated how fibers in the ALLN of goldfish, *Carassius auratus*, respond to sinusoidal water motions under different background flow conditions and whether different fiber types comparable to those found in the PLLN can be distinguished.

As a consequence of the directional sensitivity of lateral line hair cells and the innervation pattern of lateral line neuromasts (see above) about 50 % of all flow sensitive afferent lateral line nerve fibers should respond with an increase in ongoing activity to unidirectional water flow. The other 50 % of flow sensitive fibers should respond with a decrease in neural activity. In contrast to this assumption, nearly all lateral line afferents increased their discharge rates if the fish was exposed to unidirectional water flow (Carton and Montgomery, 2002; Voigt et al., 2000). Therefore it was investigated whether the responses (spike rate) of primary lateral line afferents of the goldfish, *Carassius auratus*, do change if the direction of water flow is reversed. A detailed analysis of the water flow with particle image velocimetry (PIV) and a correlation of spike train patterns with the flow characteristics was used to investigate if lateral line nerve fibers of goldfish are sensitive to d.c. flow and whether the rate increase displayed by most fibers is due to flow fluctuations that develop under flow conditions.

Up to now the lateral line system of fishes was stimulated in physiological experiments with vibrating spheres or with moving objects in both, still- and running water. In addition it was investigated how the lateral line responds to unidirectional water flow (Carton and Montgomery, 2002; Engelmann et al., 2002; Voigt et al., 2000). However, for river fish natural lateral line stimuli also include repetitive vortex motions that occur, for instance, behind inanimate objects placed in water currents (Vogel, 1996). Behavioral experiments have shown that trout make use of

these vortex motions for station holding (Sutterlin and Waddy, 1975) and for the reduction of the costs of locomotion (Liao, 2004; Liao et al., 2003a). Vortex motions are also caused by undulatory swimming fish (Blickhan et al., 1992; Cheng and Chahine, 2001; Drucker and Lauder, 1999; Linden and Turner, 2004). Piscivorous animals may use vortex motions for prey detection and hydrodynamic trail following (Dehnhardt et al., 2001; Hanke and Bleckmann, 2004; Hanke et al., 2000; Pohlmann et al., 2004; Pohlmann et al., 2001).
A specific arrangement of vortex motions is known as Kármán vortex street. A Kármán vortex street can be generated with a cylinder placed in running water (Vogel, 1996). At a Reynolds number above 40 vortices alternately detach from an upstream cylinder with each vortex rotating in a direction opposite that of its predecessor farther downstream. The frequency of vortex detachment is called vortex shedding frequency. The vortex shedding frequency VSF is a function of the Strouhal number St, which is a dimensionless index, the diameter of the cylinder d and the free stream flow velocity U (Vogel, 1996):

$$VSF = St*U/d \qquad (1)$$

The Strouhal number depends on the Reynolds number, a dimensionless index. The Reynolds number is a ratio of inertial forces (mean fluid velocity *fluid density) to viscous forces (dynamic fluid viscosity / characteristic length).
Trout align in a Kármán vortex street behind a cylinder and adjust their swimming motions to the vortex shedding frequency (Liao et al., 2003b). This raises the question whether trout (or other fish) can use lateral line information to detect the presence of a vortex street.

In this study I investigated: How lateral line fibers respond to a vibrating sphere under different flow conditions, how lateral line fibers respond to unidirectional gross water flow of different directions, and how lateral line fibers respond to a Kármán vortex street.

Materials and Methods

Experimental animals

Goldfish, ranging in length from 8 cm to 12 cm, were used for the experiments. Fish were acquired from commercial dealers and were maintained in 250-l aquaria at ambient temperature on a daily 12–12 h light-dark cycle. Prior to surgery, fish were anaesthetized with MS 222 (0.001%) and immobilized with 1–2 µl pancuronium bromide (Organon Teknika). During surgery animals were respirated with fresh water. To prevent drying of the skin, fish were permanently rinsed with fresh water. A small piece of skin was removed and the ALLN or the PLLN was exposed at its entry to the medulla by drilling a hole into the skull. To prevent water from entering the brain and to allow a complete submersion of the fish during an experiment, a plastic cylinder (diameter 12 mm) was glued on top of the skull. After surgery fish were transferred to a flow tank with one upstream and one downstream collimator, positioned on a vibration-isolated table (TMC), and fixed parallel to flow direction in a stainless-steel mouth-holder (Engelmann et al., 2002) that consisted of a mouthpiece for artificial respiration with fresh water and two screws, which kept the head in a fixed position. A cord, attached to the tail of the fish, prevented lateral movements of the fish's trunk and tail. Fish were positioned 1–1.5 cm below the water surface. To avoid inactivation of the lateral line receptors by MS 222 (Palmer and Mensinger, 2004; Späth and Schweickert, 1977), recordings were not begun until 1 h after preparation.

Generation of unidirectional water flow

All experiments were conducted in a flow tank (canal width 15 cm, water depth 16 cm, (Engelmann et al., 2002) that rested on a vibration-isolated table (TMC). Water flow was generated with a propeller (diameter 8 cm, Aeronaut) coupled to a d.c. motor (Conrad Electronic) that was driven by a power supply (Voltcraft Digi35, Conrad Electronic). The propeller was suspended from a holder on the side of the tank that was opposite to the recording section. The tank contained one upstream and one downstream flow collimator. During the experiment fish were positioned with their heads towards the flow. Flow velocity was calibrated with a flow meter

(Ott, Z200). Flow measurements were begun after the water flow reached its desired velocity and lasted for a period of 60 seconds. For these measurements the flow meter was placed at the position of the fish.

Vibrating sphere stimulus

The lateral line was stimulated with a dipole source consisting of a small (7 mm diameter) vibrating sphere attached to a vibrator (Ling, Model V101) by a stainless steel shaft (11 cm long, 2 mm diameter). The shaft was mounted perpendicular to the vibrator's diaphragm to generate sinusoidal oscillations parallel to the longitudinal axis of the fish. The vibrator was mounted to a sliding bar assembly, which allowed to manually move the dipole source parallel to the fish. To avoid boundary layer effects (Kalmijn, 1989) the distance between the surface of the sphere and the fish's skin was at least 5 mm but did not exceed 8 mm. The dipole stimulus (50 Hz) generated with the vibrator had a duration of 1 s with rise/fall times of 100 ms. Software-generated sinusoidal digital signals (Apple Macintosh, Super Scope II, GWI) were converted to analogue signals (MacAdios II, GWI, sampling rate 10 kHz), attenuated in 5-dB steps (custom-built attenuator), amplified (LDS, PA 25e) and fed into the vibrator. Peak-to-peak (p-p) displacement amplitudes of the sphere ranged between 1 µm and 350 µm. Displacement amplitudes were calibrated under a microscope (Leitz, Dialux) in air.

Data acquisition

Neural activity of ALLN or PLLN fibers was recorded with glass micropipettes filled with 3 mol/l KCl (impedance 50–90 MΩ). Electrodes were placed on the nerve with a motorised microdrive (Nanostepper MPC, Science Products Trading) and advanced with a micromanipulator. Action potentials were amplified (VF 180, Biologic), low-pass filtered (cut-off frequency 1 kHz or 10 kHz), displayed on an oscilloscope (Yokogawa DL-1800 A) and stored online (Superscope II). During experiments, neural activity was monitored with a loudspeaker (audio monitor). All units were tested for their responses to water movements created by moving a handheld pipette through the tank, or to small water jets that were generated by the pipette and directed to the skin of the fish. Units that did not respond to these

water motions were excluded from further investigations. Many of the responsive fibers were lost before the entire stimulus protocol could be completed. For this reason, the sample size for different stimulus conditions varies.

Data analysis

Recordings were filtered off-line (high-pass 100 Hz, low pass 3 - 5 kHz) and spikes were separated from background noise. Data analysis was carried out with self-written scripts in Igor Pro 4 (Wavemetrics Inc). If not otherwise stated the values reported herein are mean values ± standard deviation.

Flow sensitivity

To be able to compare the data from the ALLN with those obtained from the PLLN fibers were classified according to the criteria introduced by Engelmann et al. (2000, 2002). Consequently, fibers were classified as flow sensitive (type I) if ongoing discharge rates obtained in still water were significantly different (Wilcoxon signed-rank test, $p \leq 0.01$) from those in a water flow of 10 $cm*s^{-1}$. Fibers were classified as flow insensitive (type II) if discharge rates in still and running water (10 $cm*s^{-1}$) were comparable.

Vibrating sphere

Responses to the vibrating sphere were quantified by the average discharge rates (spikes per second) during sphere vibration and the degree of phase locking (synchronization coefficient R) (Goldberg and Brown, 1969). Average discharge rates were determined from the number of spikes elicited during the 10 stimulus presentations and expressed in spikes per second. Evoked spike rates were compared with ongoing discharge rate measured one second prior to stimulus onset. To determine the degree of phase locking, elapsed spike times across all stimulus presentations were added and collapsed into a single cycle's worth of time (period histogram). The Rayleigh statistic $Z=n*R^2$ was used to determine whether measures of phase locking were statistically significant, where n is the

number of spikes (Batschelet, 1981). Z values above 4.6 indicate a probability of 0.01 or less that spikes were randomly distributed during a vibration cycle. Level-response functions for evoked spike rates (ongoing activity subtracted) and for synchronization coefficients obtained in still and running water were compared by analysis of covariance (ANCOVA, $p \leq 0.05$). Responses were classified as masked if the slope of the regression line of a response function obtained under flow conditions was significantly smaller than the slope of the response function obtained in still water, or if the response functions were shifted along the y-axis (ANCOVA, $p \leq 0.05$). To determine the degree of masking, level-response functions for both spike rates (ongoing activity subtracted) and synchronization coefficients were integrated. Integrals of response functions obtained in running water were expressed as percent of the integrals of the response functions obtained in still water (Engelmann et al., 2002).

Particle Image Velocimetry (PIV)

A high speed PIV system (LaVision, Highspeedstar 4) was used to visualize and quantify water motions (Chagnaud et al., 2006). Neutrally buoyant particles (LaVision, Sphericel 110P8) - suspended in the water - were illuminated with a light sheet (<1 mm thick) that was generated with a laser. The light sheet was oriented parallel to the lateral surface of the fish. Due to the head, dorso-ventral and rostro-caudal curvatures of the fish and laser light reflections on the fish surface it was not possible to align the laser sheet directly at the fish surface.
Individual pictures were taken at a frame rate of 250 Hz, i.e., the temporal precision of the PIV was 4 ms. Construction of PIV-images (vector plots) was performed with the software Davis 7 (LaVision). Successive frames were analyzed by time series sequential cross-correlation with an interrogation window-size of 256*256 pixel (16*16 vectors). To improve the analysis, an overlap between neighboring interrogation windows was applied which resulted in a final window-size of 128*128 pixel (32*32 vectors). Application of a multi-pass filter further reduced the error of the calculated vectors. This filter executed iterative (n=1) evaluations of the same pair of images. In the first pass a vector was computed and used as a reference for the following pass. In the second pass the

interrogation window of the first frame was shifted by half the amount of the reference vector and in the opposite direction while the interrogation window of the second frame was shifted in the direction by half of the amount of the reference vector. Thus, the correlation in the second pass anticipates the main motion direction of the particles and adjusts the interrogation area such that the maximum number of particles is included. This enhances the precision of the PIV. Finally a median filter was used to compute the median vector for eight neighboring interrogation windows. If the centre vector (surrounded by the eight interrogation windows) differed from the median vector by more than 3 times the root-mean-square, the centre vector was replaced by the averaged vector obtained from the neighboring interrogation windows. After the computation the vector plots were post-processed. The same median filter and smoothing was used as during the computation of the vector plots.

Experimental protocols and special analysis

I Responses of ALLN fibers to dipole stimuli

Experimental protocol

To measure the ongoing discharge rate of a fiber, the non-vibrating sphere was placed at least 10 cm behind the fish and neural activity was recorded in still water for 60 s (10 consecutive trials of 6 s duration each). To determine neural activity in running water, this protocol was repeated with the water flow set to 10 $cm*s^{-1}$. Neural activity in response to the vibrating sphere was recorded with the sphere placed in the centre of the receptive field (RF) of a fiber. RF centre was determined by moving the vibrating sphere (Frequency: 50 Hz, peak to peak amplitude: 30 µm) slowly along the side of the fish in a head-to-tail or tail-to-head direction. The sphere was then placed at the location from which the strongest responses, judged by listening to the audio monitor, were elicited. This method was used previously and allowed to determine the RF centre in the horizontal plane with a precision of 0.1 ± 1.2 cm (Chagnaud et al., 2006). With the sphere at the RF centre, level-

response functions were measured in still and running water (flow velocities 6.5, 10 and 13.5 cm*s^{-1}). For each displacement amplitude, stimuli were presented ten times with inter-stimulus time intervals of 5 s.

II Responses of lateral line fibers to running water

Experimental protocol

The lateral line was stimulated with unidirectional water flow (0, 4, 6.5, 8, 10, 12, 13.5, 15 cm*s^{-1}). The direction of water flow usually was from anterior to posterior, but in some experiments the direction of water flow was reversed. Ongoing activity under still water and - in discrete steps (see above) - under running water conditions was recorded for 60 s (in some experiments 30 s). Care was taken that the flow reached the desired velocity before recording the neural activity. After completion of the stimulus protocol the flow was turned off. Each stimulus protocol was repeated up to 3 times.

Detailed data analysis

Peri-stimulus-time histograms (PSTH), raster plots and Fast Fourier transformations (FFT) of the spike trains were computed. For each fiber the instantaneous frequency (IF) was calculated as the reciprocals of the inter spike time intervals. Thereafter the average spike frequency of that fiber was subtracted from all IF values and calculated the root mean square (RMS) value of the resulting curve. The RMS value was expressed as percent of the average spike rate measured under still water conditions. Thus, the RMS value is a measure for the variability of the IFs obtained at the different flow velocities. For each fiber the average ongoing rate (still water and running water conditions) was determined either in absolute values or as the difference between the rates obtained at different flow velocities (0 - 15 cm*s^{-1}).

A fiber was defined as flow sensitive if its discharge rate, measured under still water conditions, was significantly different from its discharge rate measured under running water conditions (Wilcoxon test, significance level $p \leq 0.01$). Depending on flow velocity the same fiber could be flow sensitive or flow insensitive. To test for flow sensitivity the flow velocities of 6.5, 10 and 13.5 cm*s^{-1} were apllied. Linear regressions of the flow velocity functions of the fibers were computed (Excel,

Microsoft). Coefficients of determination $R^2 \geq 0.6$ were used to determine whether there was a correlation between discharge rate and flow velocity.
For the analysis the instantaneous frequencies IF (reciprocals of the inter spike intervals) and the fast Fourier transformation (FFT) of the spike trains were computed. To compare the variability of primary afferent discharges the mean IF of each fiber was subtracted from each instantaneous frequency value of that fiber. Thereafter the root mean square (RMS) value for each fiber was calculated, i.e. a value that can be used as a measure for firing variability. The RMS value is a statistical measure of the magnitude of a varying quantity. It can be calculated for a series of discrete values or for a continuously varying function.

$$\text{RMS} = \sqrt{\frac{1}{N}\sum_{i=1}^{N} x_i^2} \qquad (2)$$

III Responses of lateral line fibers to a Kármán vortex street

To generate a vortex street a cylinder (diameter 2.5 cm, length 20 cm) was placed vertically at a distance of 20 cm upstream to the fish (Fig. 1). Perpendicular to the flow direction the position of the cylinder was varied. At position p_0, it was directly ahead of the fish. At the positions p_1, p_2 and p_3 the cylinder was moved laterally by 2, 4 and 6 cm, respectively.

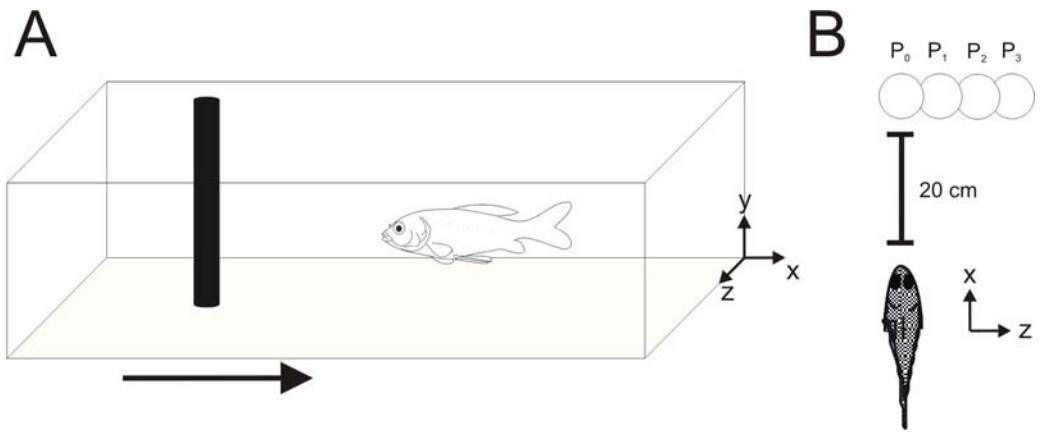

Fig. 1: Part of the flow tank (A) with a cylinder (not to scale) that generated the vortex street. Black arrow below the tank indicates the direction of water flow. B Dorsal view of the fish with the cylinder placed at the positions p_0 – p_3. The drawing is not to scale.

To alter the vortex shedding frequency either the free stream flow velocity (6.5, 10 and 13.5 cm*s^{-1}) was changed or the cylinder diameter (1.0, 2.5 and 7.8 cm). Vortex shedding frequency was calculated using a Strouhal number of 0.2 (Vogel, 1996). The Reynolds number was calculated according to the formula (Vogel, 1996):

$$Re = \rho * V * D * \mu^{-1} \qquad (3)$$

V = free stream fluid velocity V (6.5, 10 and 13.5 cm*s^{-1}), D = characteristic distance (canal width = 15 cm), ρ = fluid density (0.998 kg*m^{-3}), μ = fluid viscosity (1.002 Pa*s^{-3}). The Reynolds number varied between 1000 and 20000 depending on the flow velocity applied. Ongoing activity was recorded for 60 s under still water (SW), running water (RW, 10 cm*s^{-1}) and Kármán vortex street (KVS) conditions, respectively.

Results

I Responses of ALLN fibers to dipole stimuli

Single unit recordings were made from 243 fibres in the right (ipsilateral) ALLN of goldfish (N=22). Of these, 220 responded to hydrodynamic stimuli (unidirectional water flow, sinusoidal water motions or, water motions generated by moving a pipette in the experimental tank) with a change in discharge rate and/or discharge pattern. The remaining 23 fibres did not respond to any of these stimuli and were thus not further investigated. The average ongoing activity of the 220 responsive fibres under still water conditions was 26.6 ± 21.0 spikes*s^{-1} (mean ± SD, median: 23.3 spikes*s^{-1}).

Classification of fibres

Ongoing activity of 153 fibres was recorded in still water and in a 10 cm*s^{-1} water flow. 119 of these fibres were flow sensitive, i.e., in each of these fibres the discharge rate in running water differed from that in still water (Wilcoxon signed-rank test: $p \leq 0.01$). These fibres were classified as type I fibres. The remaining 34 fibres were not sensitive to unidirectional water flow, i.e., discharge rates in running water were not different from those in still water (Wilcoxon signed-rank test, $p > 0.01$). These fibres were classified as type II fibres.

On average, ongoing activities of type I fibres in still water (mean 27.2 ± 25.5 spikes*s^{-1}) were not different from the still water rates of type II fibres (mean 26.9 ± 18.7 spikes*s^{-1}) (Mann-Whitney U-test, p=0.64). In contrast, in running water ongoing activities of type I fibres (mean 43.6 ± 25.0 spikes*s^{-1}) were significantly greater than those of type II fibres (mean 27.2 ± 20.0 spikes*s^{-1}) (Mann-Whitney U-test, p=0.004).

In a separate experiment, fluctuations were introduced into the flow by placing a cylinder (2.5 cm diameter, 20 cm length) vertically into the tank at a distance of 20 cm in front of the fish. The cylinder was positioned either directly ahead of the fish (p_0) or 2 cm (p_1) or 4 cm (p_2) displaced to the right. A cylinder in a flow sheds predictable vortices, thus generating a Kármán vortex street (Vogel, 1996). The discharge rates of 37 ALLN fibres were recorded in flow with the cylinder placed at one of the three positions and compared with those recorded in flow without a cylinder. There was no difference in discharge rate between these conditions. Average discharge rates were 40.15 ± 19.4 spikes*s^{-1} (n=37) in flow without a cylinder, 36.5 ± 20.5 spikes*s^{-1} (n=37) in a flow with the cylinder at p_0 (Mann Whitney U-test, p=0.35), 30.7 ± 25.5 spikes*s^{-1} (n=19) with the cylinder at p_1 (p=0.08) and, 38.7 ± 20.8 spikes*s^{-1} (n=24) with the cylinder at p_2 (p=0.84). Discharge rates for the different cylinder positions were also not different from each other (Mann Whitney U-test, p_0 vs. p_1: p=0.21, p_0 vs. p_2: p=0.56, p_1 vs. p_2: p=0.19). Thus it was not possible to determine from the discharge rates if a cylinder was in the flow and at which of the three positions.

Responses to dipole stimuli in still water

Responses to sinusoidal water motions were obtained from 72 fibres. All fibres exhibited phase locked, tonic discharges in response to the sinusoidal vibration (Fig. 2A, 3A). At stimulus levels near threshold, fibres responded with a modulation of ongoing activity, i.e. they exhibited phase locking with no or little increase in discharge rate (Fig. 2C, 3C). Both, degree of phase locking and discharge rate increased with increasing displacement amplitude. In 35 fibres, particularly at high displacement amplitudes, a period of decreased neural activity was observed after the stimulus ended (e.g., Fig. 3A). At the highest displacement amplitudes used, the number of spikes generated per wave cycle increased up to 4 spikes per cycle which resulted in a decrease in phase locking in 24 fibres.

Responses to dipole stimuli in a 10 cm*s^{-1} water flow

Of the 72 fibres from which responses to dipole stimuli were obtained, 63 were classified as type I fibres and nine as type II fibres. The responses of 41 of the 63 type I fibres were masked by a 10 cm*s^{-1} water flow. In 16 fibres, responses were masked both in terms of evoked spike rate and in terms of phase locking (see Fig. 2), in 15 type I fibres, responses were masked only in terms of evoked spike rate and, in 10 type I fibres responses were masked only in terms of phase locking. The responses of 22 fibres classified as type I were not masked by a 10 cm*s^{-1} water flow. An example of a fibre whose response was masked in running water is shown in Fig. 2. In running water, the ongoing activity of this fibre increased (compare ongoing rates in Fig. 2B). Consequently, level response functions measured in running water were shifted to lower values compared to those measured in still water (compare Figs. 2C and D).

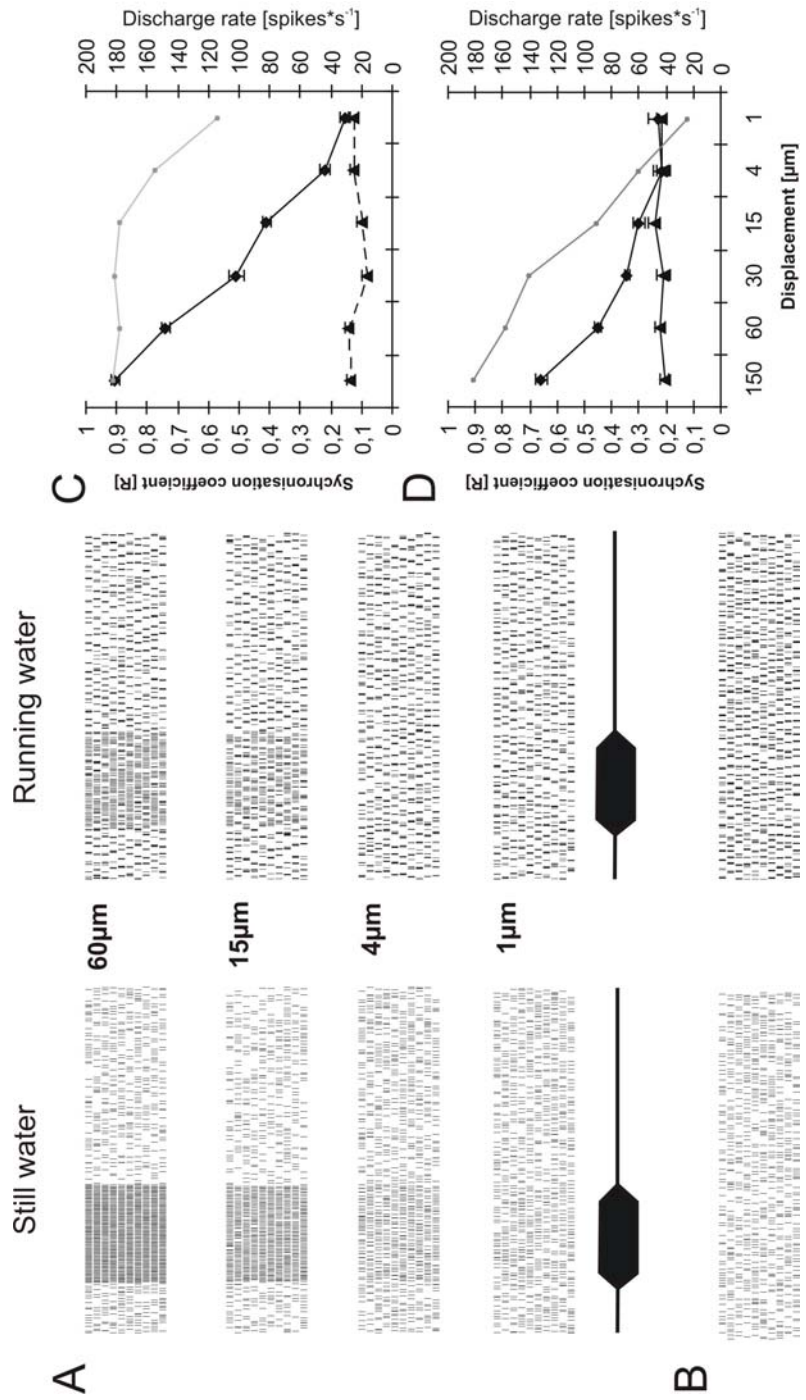

Fig 2: Responses of a type I ALLN fiber of the goldfish to a 50 Hz vibrating sphere stimulus applied under still (left) and running (right) water (10 cm*s^{-1}) conditions. A, Raster plots of the responses to 10 stimulus presentations with displacement amplitudes of 1 µm, 4 µm, 15 µm and 60 µm. Each marker represents one action potential. The stimulus traces are shown below the raster plots. B, Raster plots of the activity of the fiber in still and running water without sphere vibration. C, D Level response functions obtained in still water (C) and running water (D). Evoked discharge rates (mean ± S.D.) (circles) averaged across 10 stimulus presentations, ongoing discharge rates (triangles) and synchronization coefficients (grey lines connecting small symbols) are plotted as function of sphere displacement.

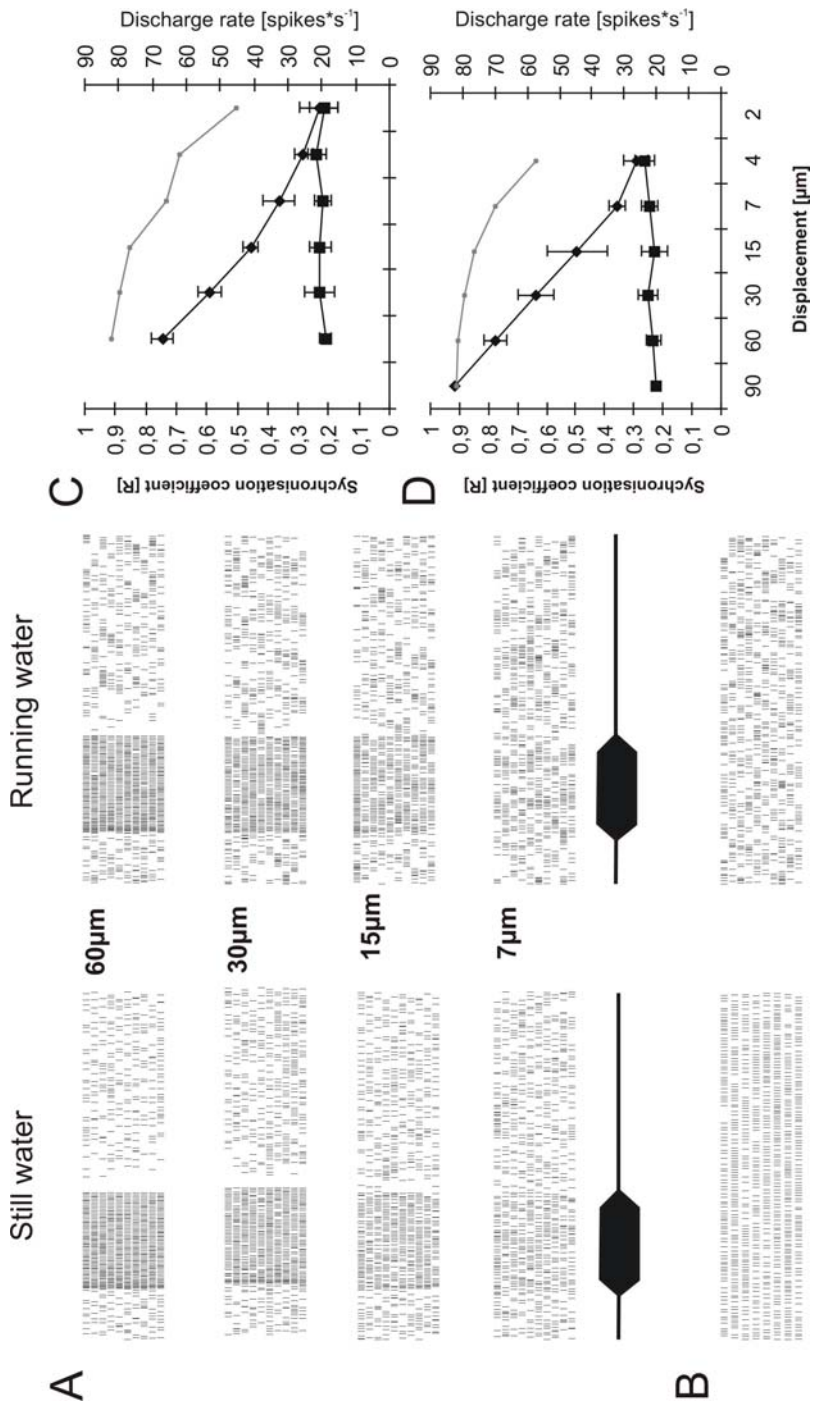

Fig 3: Responses of a type II ALLN fiber of the goldfish to a 50 Hz vibrating sphere stimulus applied still (left) and running (right) water (10 cm*s^{-1}) conditions. A, Raster plots of the responses to 10 stimulus presentations with displacement amplitudes of 7 µm, 15 µm, 30 µm and 60 µm. Each marker represents one action potential. The stimulus traces are shown below the raster plots. B, Raster plots of the activity of the fiber in still and running water without sphere vibration. C, D Level response functions obtained in still water (C) and running water (D). Evoked discharge rates (mean ± S.D.) (circles) averaged across 10 stimulus presentations, ongoing discharge rates (triangles) and synchronization coefficients (grey lines connecting small symbols) are plotted as function of sphere displacement.

The responses of 7 out of the 9 type II fibres were masked by running water neither in terms of evoked spike rates, nor in terms of phase locking (for an example see Fig. 3). In one type II fibre, the evoked spike rate but not phase locking, and, in another type II fibre, phase locking but not the evoked spike rate was masked in running water.

The degree of masking of type I and type II fibers was measured by comparing the integrals of the level-response functions in still and running water and the results are shown in Fig. 4. For type I fibres, averaged integrals of the rate functions in running water were 55.2% (range 0.4 – 131.6 %) of those in still water (100%). Averaged integrals of the phase locking functions were 80.6% (range 13.8 – 123.4 %) of those in still water. Thus, across the population of type I fibres, responses to the vibrating sphere were masked in terms of evoked spike rates and, although to a smaller degree, in terms of phase locking. For type II fibres, averaged integrals of the rate functions in running water were 94.2 % (range 33.7 – 139.1 %) of those in still water. These values were significantly different from those obtained from type I fibres (Mann Whitney U-test, $p=0.001$). Averaged integrals of the phase locking functions of type II fibres were 92.7 % (range 83.8 - 103.0 %) of those in still water. These values were barely different from those obtained from type I fibres (Mann Whitney U-test, $p=0.078$). Thus, in contrast to type I fibres, responses of type II units were masked neither in terms of evoked spike rate nor in terms of phase locking.

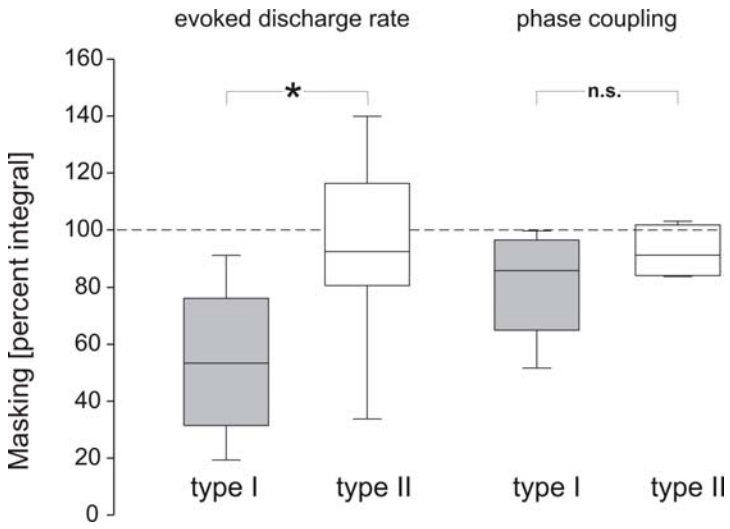

Fig 4: Summary of the characteristics of type I and type II fibers of goldfish. Box-and-whisker plots are shown representing median values and 10th, 25th, 75th and 90th percentiles. The integrals of the level response functions for evoked activity (gray bars) and for the degree of phase locking (white bars) are expressed as percentage of the integrals of the response functions measured in still water. Asterisk indicates statistically significant differences (U-test, p=0.001). n.s., no significant difference (p=0.078).

Responses to dipole stimuli at different flow velocities

To determine the effect of different flow velocities on lateral line responses the responses to sinusoidal water motions that were presented in a 6.5, 10 and 13.5 $cm*s^{-1}$ water flow were recorded. The results show that for both type of fibres, the ratio between masked responses and responses that are not masked increased systematically with increasing flow velocity. For type I fibres, the responses that were masked in terms of evoked discharge rates increased from 52% (n=15 out of 29) at 6.5 $cm*s^{-1}$ to 76% (n=22 out of 29) at 10 $cm*s^{-1}$ and to 90% (n=17 out of 19) at 13.5 $cm*s^{-1}$ flow velocity (Table 1). The responses that were masked in terms of phase locking increased from 10% (n=3 out of 29) at 6.5 $cm*s^{-1}$ to 41% (n=12 out of 29) at 10 $cm*s^{-1}$ to 63% (n=12 out of 19) at 13.5 $cm*s^{-1}$ flow velocity (Table 1). Similarly, the proportion of masked responses of type II fibres also increased with

increasing flow velocity both in terms of discharge rate and in terms of phase locking. However, the number of type II fibres investigated was low (n=4).
Fig. 5 shows level response functions for rate and phase locking of type I fibres, at different flow velocities. In 19 out of 27 type I fibres from which complete level responses functions at all three flow velocities could be obtained, the degree of masking for both evoked rates and phase locking increased with increasing flow velocity, resulting in a shift of the response functions towards lower values (Fig. 5A). The responses of 5 type I fibres were affected only in terms of phase locking. In these fibres increasing flow velocities caused a systematic shift in the phase locking functions whereas the rate response functions were not affected (Fig. 5B). In 3 type I fibres, responses were masked neither in terms of evoked spike rates nor in terms of phase locking at any of the flow velocities applied (Fig. 5C).

Table 1: Proportions of type I and type II ALLN fibre responses to sinusoidal wave stimuli that were masked and those that were not masked in running water at different flow velocities.

	*Velocity [cm*s^{-1}]*	*6.5*	*10*	*13.5*
Evoked activity	type I masked/not masked	15 / 14	22 / 7	17 / 2
	type II masked/not masked	1 / 3	1 / 3	2 / 3
Phase locking	type I masked/not masked	3 / 26	12 / 17	12 / 7
	type II masked/not masked	0 / 4	0 / 4	1 / 2

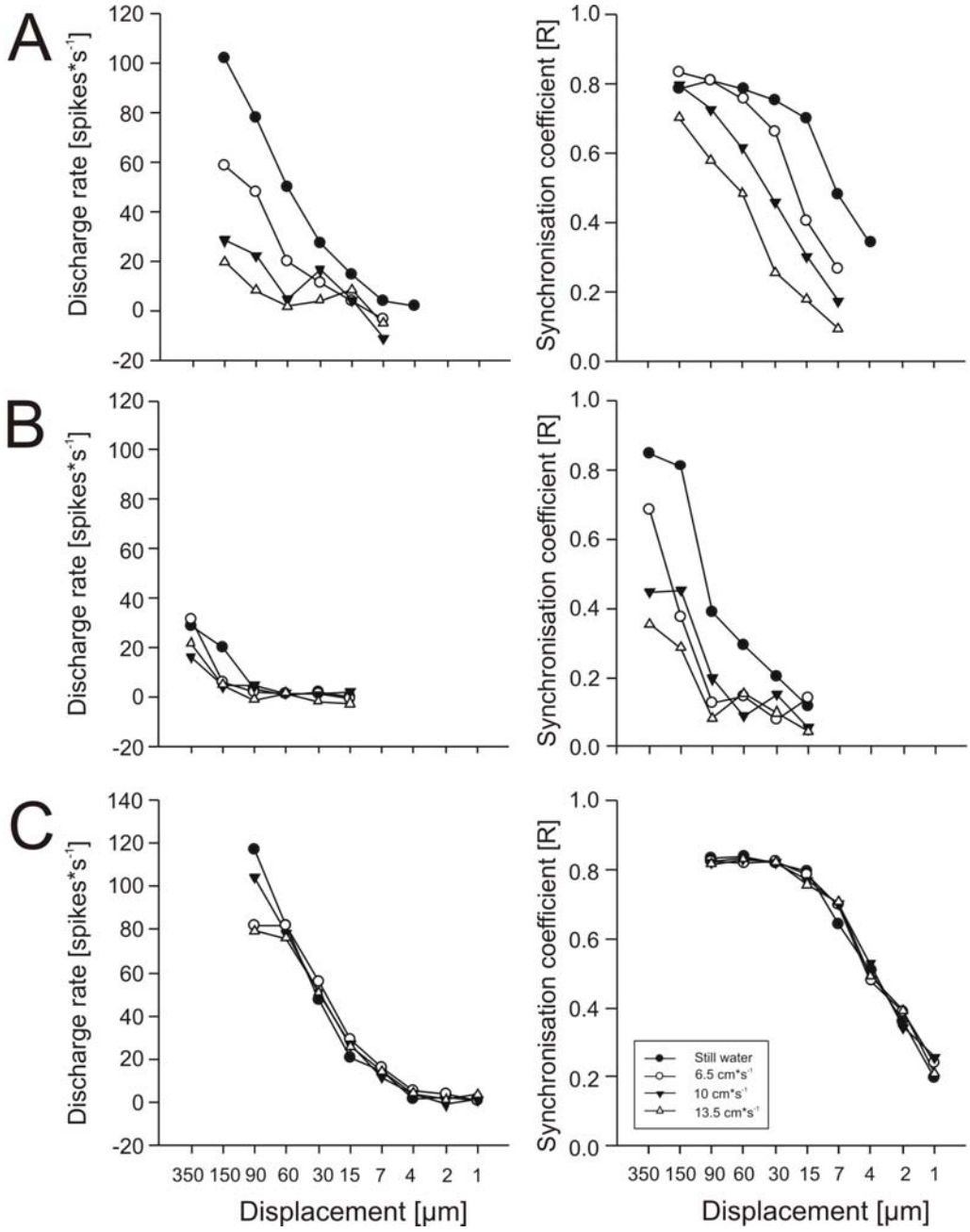

Fig 5: Level-response functions of three representative type I fibers. Fibers were tested in still water (filled circles) and in running water (6.5 (circles), 10 (filled triangles) and 13.5 cm*s^{-1} (triangles)). Discharge rates (left column) and synchronization coefficients (right column) are plotted as function of sphere displacement. A. Response functions of a type I fiber whose responses to the dipole stimulus were masked in running water both in terms of discharge rate and in terms of phase locking. Note that level-response functions were shifted systematically with increasing flow velocity, i.e., the degree of masking increased with increasing flow velocity. B. Response functions of a type I fiber whose responses were masked in terms of phase locking but not in terms of evoked discharge rates. C. Response functions of a type I fiber whose responses were not masked in running water.

Fig. 6 shows level response functions for rate and phase locking from a type II fibre at different flow velocities. Complete response functions at three flow velocities were recorded from 3 type II fibres. The responses to the dipole of each of these fibres were not masked at any of the applied flow velocities, neither in terms of evoked spike rates nor in terms of phase locking.

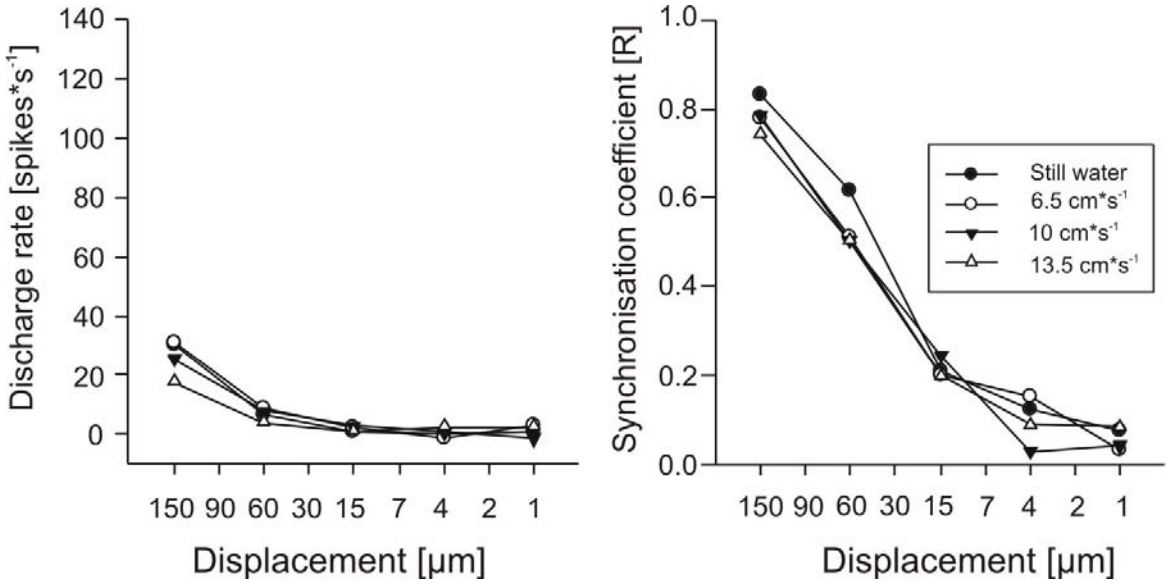

Fig 6: Level-response functions of two representative type II fibers measured in still water and in running water (6.5, 10 and 13.5 cm*s^{-1}). Discharge rates (left column) and synchronization coefficients (right column) are plotted as function of sphere displacement. A. Response functions of a type II fiber whose responses to the dipole stimulus were not masked in running water.

The degree of masking of dipole-evoked responses at different flow velocities is shown in Fig. 7. Here, the percentages of the integrals of the level response functions for both evoked activity and phase locking are plotted as a function of flow velocity (integrals in still water = 100%). Despite the large variability, the data indicate that the degree of masking increased, i.e., percent integrals decreased, with increasing flow velocity. In some fibres (n=8 for evoked activity and n=7 for phase locking), the degree of masking decreased (increasing percent integrals) in running water, however only at the lowest flow velocity amplitude applied (6.5 cm*s^{-1}).

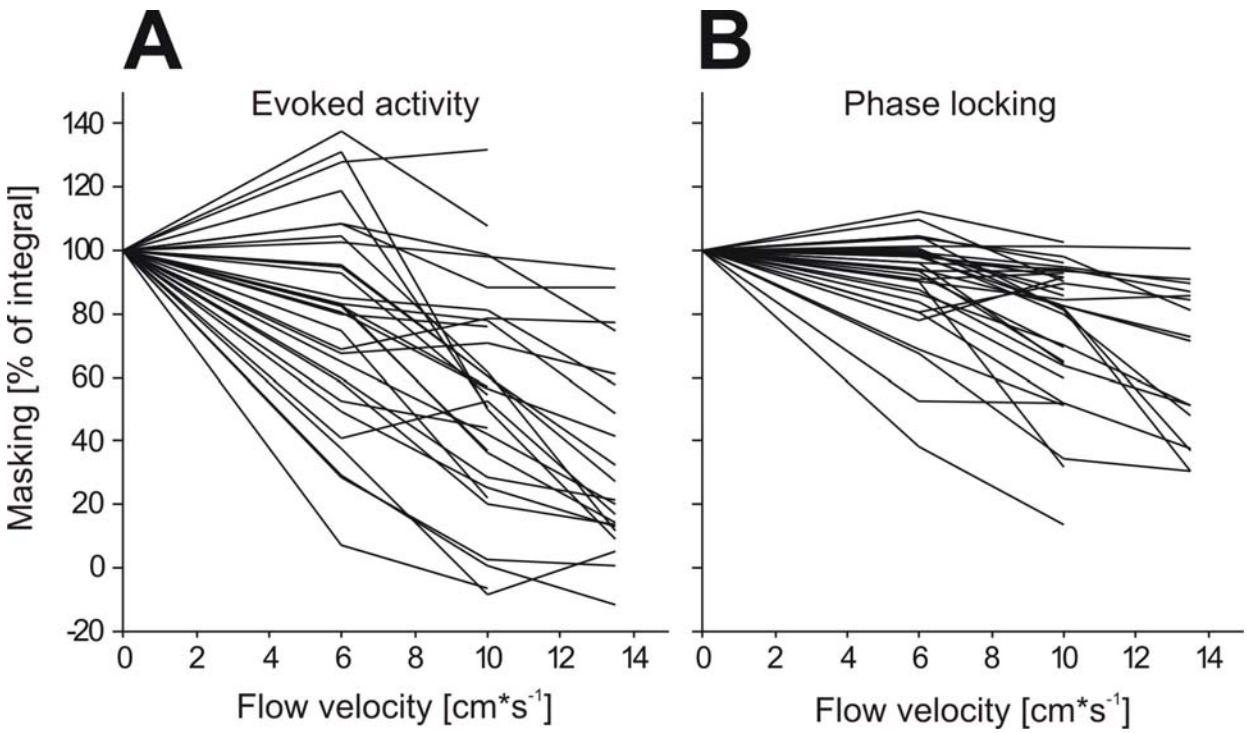

Fig 7: Degree of masking of dipole evoked responses by running water. Percent integrals of the level-response functions obtained in running water relative to those obtained in still water (100%) are plotted as function of flow velocity for spike rates (A) and synchronization coefficients (B).

Responses to dipole stimuli in turbulent flow

To investigate the effects of flow fluctuations, the responses of 19 type I and 5 type II fibres to sinusoidal water motions in a flow with a cylinder placed at position p_0, p_1 or p_2 in the experimental tank were recorded and compared with responses obtained in flow without a cylinder and with those obtained in still water. From these data, a differential effect of the different flow conditions on the responses to the vibrating sphere was not apparent. For type I fibres the degree of masking was comparable for each flow condition (e.g., see Fig. 8A). For type II fibres, the response functions obtained under the different flow conditions were comparable to those obtained in still water, i.e., responses were not affected by any of the flow conditions applied (e.g., see Fig. 8B).

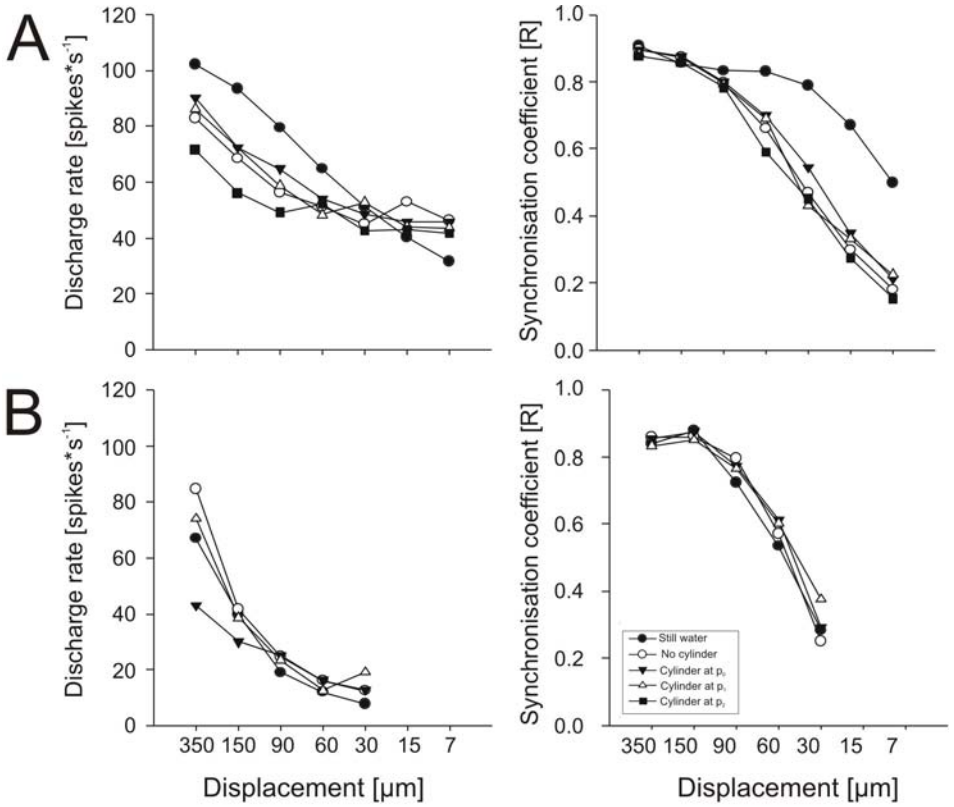

Fig 8: Level-response functions of a type I fiber (A) and a type II fiber (B) in still water and in a 10 cm*s^{-1} water flow without and with a cylinder at different locations (p_0, p_1, p_2) in the experimental tank. Discharge rates (left column) and synchronization coefficients (right column) are plotted as function of sphere displacement. Note that the response functions recorded in flow were shifted relative to those obtained in still water by about the same degree irrespective of the different flow conditions.

Stimulus measurements

The PIV method was used to characterize the water motions generated by running water with and without a cylinder in the flow and the water motions generated by a stationary vibrating sphere in still and running water. For these measurements a vertically oriented laser sheet was placed at the position that was usually occupied by the fish.

Running water. Vector plots of the water motions as well as the average and the RMS velocity of a 10 cm*s^{-1} flow in the absence and in the presence of a cylinder are shown in Fig. 9. Without a cylinder, the water flow within the window covered by the camera was uniform, i.e., all water particles moved with comparable velocity

in the same direction. Thus, the corresponding vectors were of comparable length and had an identical orientation (Fig. 9A upper left). However, vector plots that were calculated from two consecutive frames revealed that the flow in the experimental tank was not perfectly laminar but subject to some velocity fluctuations (different colours in Fig 9A). To estimate mean flow velocity flow vectors across 2048 frames were averaged (i.e., 8.2 seconds, frame rate 250 Hz). The resulting vector plots revealed a systematic distribution of water velocities along the vertical axis of the tank: velocity decreased with increasing distance from the water surface (Fig 9B centre left). To obtain an estimate of the variability of the velocity fluctuations at each point in space the average flow velocity from each vector was subtracted and the RMS values (see materials and methods) were calculated. For a flow without a cylinder these fluctuations were fairly small (Fig. 9C lower left).

If a cylinder was placed in the flow the flow field was less uniform (Fig. 9 A). Moreover, vector plots as well as average and RMS velocity showed fluctuations that depended on the position of the cylinder relative to the plane of observation, i.e. the location of the fish. If the cylinder was in at p_0, flow velocity was lower (on average) and velocity fluctuations (RMS of flow velocity) were greater than without a cylinder. The more the cylinder was moved out of the plane of observation, the greater were the absolute flow velocities In contrast, velocity fluctuations decreased in amplitude, i.e., the flow became more uniform (compare vectors and background colours for p_0, p_1 and p_2 in Fig. 9A). These changes are also evident if one compares average and RMS velocities. If the cylinder was at p_0, average flow velocity was lowest and even lower than the average flow velocity without cylinder. Average flow velocity increased systematically with increasing lateral distance of the cylinder but was still lower than without a cylinder even if the cylinder was placed at p_1 or p_2 (compare p_0, p_1 and p_2 in Fig. 9B). RMS velocities with a cylinder were always greater than those without a cylinder and decreased with increasing lateral distance of the cylinder (Fig. 9C). These findings demonstrate that in these experiments the lateral line of the fish was subject to different flow conditions both, in terms of absolute velocities and in terms of velocity fluctuations depending on whether or not a cylinder was in the tank and on the relative position of cylinder and fish.

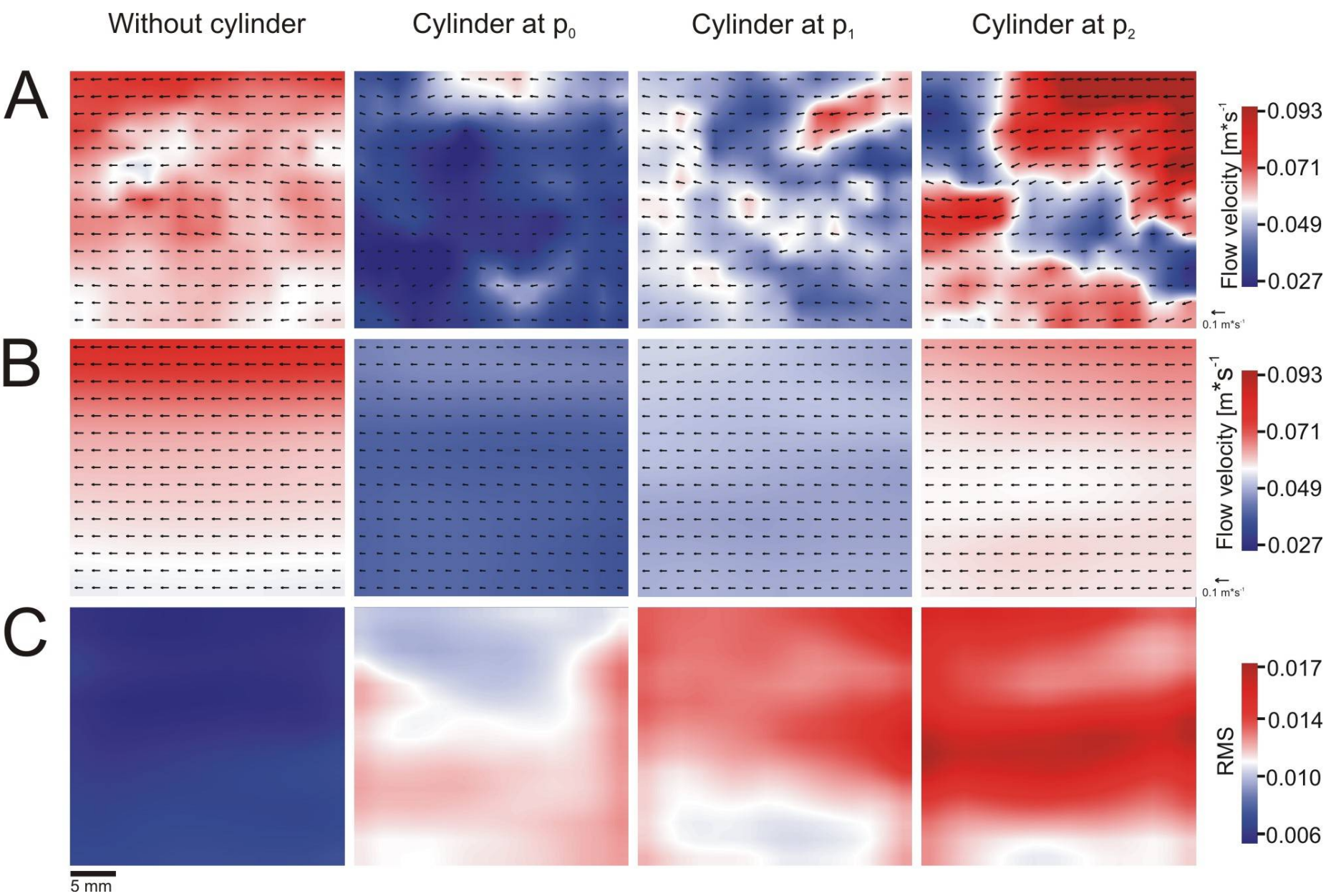
Without cylinder
Cylinder at p_0
Cylinder at p_1
Cylinder at p_2
A
B
C
Flow velocity [m*s^{-1}]
0.093
0.071
0.049
0.027
0.1 m*s^{-1}
RMS
0.017
0.014
0.010
0.006
5 mm

Fig. 9: The water flow associated with the different flow conditions used in the experiments. A. Vector plots on a laminar flow and on a flow that was disturbed by a cylinder placed at p_0, p_1 and p_2 (see Methods). Background colors code for water velocity. Vectors were obtained by comparing two consecutive frames. B. Vector plots obtained by averaging across 2048 consecutive frames. C. RMS velocity (average water velocity subtracted) obtained from 2048 consecutive frames. Frame rate in A, B and C was 250 Hz.

Dipole stimulus. The water motions produced by a sphere that vibrated with 50 Hz in still and running water are shown in Fig.10. The sphere was located in the centre of each image, 5 mm behind the plane of observation (behind the laser sheet). The vibration axis was tilted by about 25° relative to the horizontal plane.

Under still water conditions (Fig. 10A), the water motions generated by the vibrating sphere were clearly visible in the vector diagrams. When the sphere was displaced from left to right, water moved around the sphere resulting in vectors that were, in the plane of observation, pointing from right to left (Fig. 10A, 1st and 2nd image). Reversal of the motion direction of the sphere resulted in vectors that were pointing in the opposite direction (Fig. 10A, 3rd and 4th image). Just before the sphere was maximally displaced, the vector lengths decreased due to the reduced velocity of the sphere (Fig. 10A, 5th image).

If the sphere was exposed to running water (10 cm*s^{-1}) (Fig. 10B), the sinusoidal water motions generated by the vibrating sphere no longer showed up in the vector diagram. In each image, vectors had comparable length and were pointing from right to left, i.e., they represented the direction of bulk water flow that masked the sinusoidal water motions generated by the sphere. To visualize the dipole-generated water motions in running water, the average vector length, obtained from all vectors of 100 frames (i.e., across 400 ms) of flow, was subtracted from each vector (Fig. 10B). The resulting vector plots showed a great similarity with those obtained under still water condition (compare Fig. 10C with Fig. 10A), demonstrating that it is possible to reconstruct the water motions caused by a sinusoidally vibrating sphere even if these water motions are masked by running water.

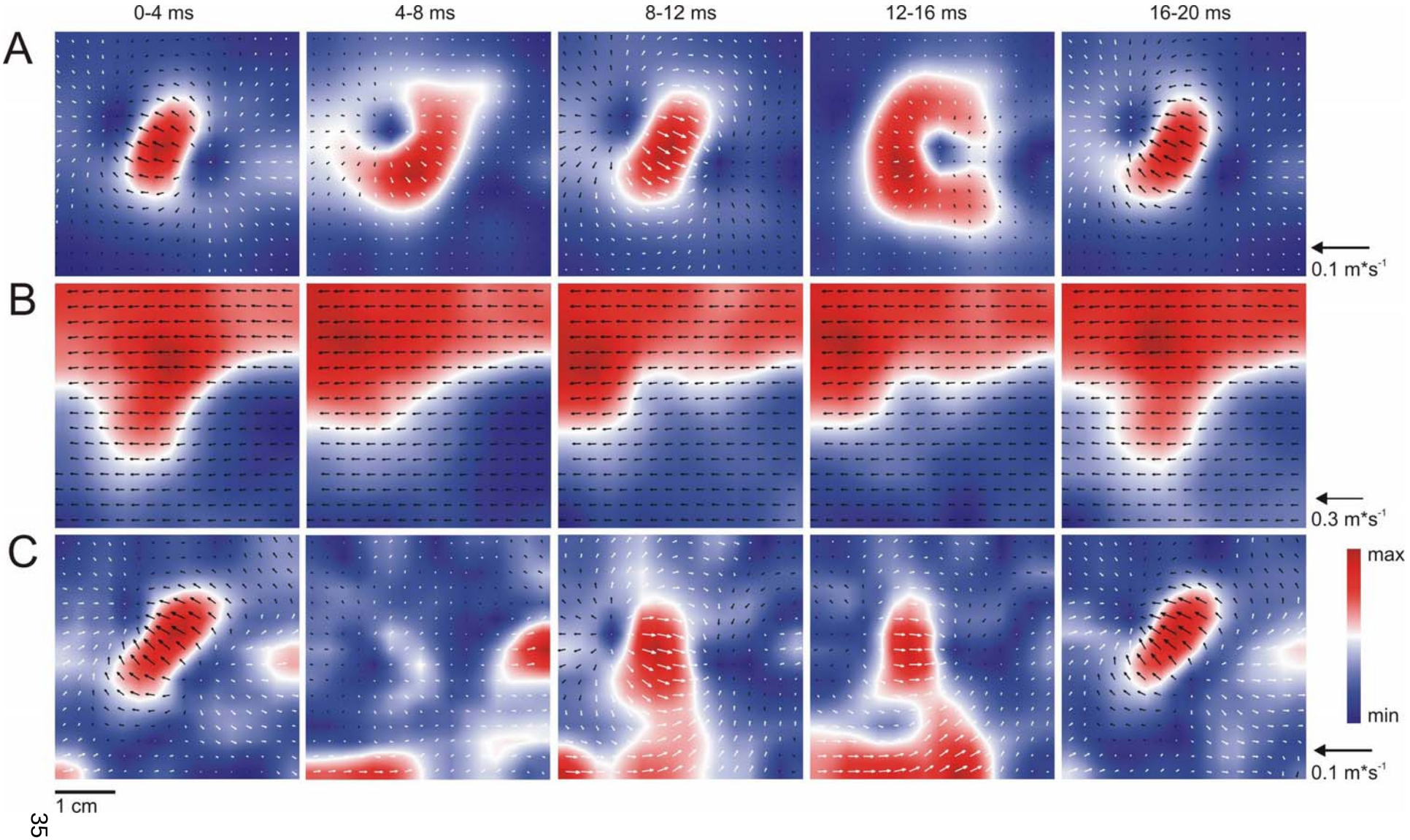
0-4 ms
4-8 ms
8-12 ms
12-16 ms
16-20 ms
A
B
C
0.1 m*s-1
0.3 m*s-1
max
min
0.1 m*s-1
1 cm

Fig 10 A-C: Vector plots representing the water motions generated by a dipole stimulus. Images were recorded at a frame rate of 250 Hz. Time intervals are indicated on top. Vectors represent the direction (vector orientation) and the velocity (vector length) of (water) particle movement. Reference vectors are given at the right of each sequence. Vectors pointing from left to right are shown in white, vectors pointing from right to left are shown in black. Background colors represent the range of vector lengths observed in each image. Due to the limitations of the camera optics, a sphere of 15 mm diameter was used for these measurements. A Vector plots of the water flow generated by a sinusoidally vibrating sphere (50Hz, 150 µm peak-peak displacement) in still water. B Vector plots of the water flow generated by the sinusoidally vibrating sphere in running water (10 $cm*s^{-1}$ flow velocity). C Same as B, however, the vector that was obtained by averaging across 100 frames of flow was subtracted.

II Responses of lateral line fibers to running water

Flow sensitivity of anterior lateral line nerve fibers

The responses of 42 ALLN fibers to unidirectional water flow were recorded. Under still water conditions ongoing activity was 30.8 ± 20.9 $spikes*s^{-1}$ (mean ± SD; median: 28.5 $spikes*s^{-1}$). At a water velocity of 6.5 $cm*s^{-1}$, 30 out of the 42 fibers were flow-sensitive, i.e. these fibers either significantly increased (25 fibers) or decreased (5 fibers) their discharge rates. Twelve fibers were flow insensitive. However, if flow velocity exceeded 6.5 $cm*s^{-1}$, more and more of these fibers became flow sensitive (Tab. 2). In addition, fibers that responded with a decrease in ongoing activity at 6.5 $cm*s^{-1}$ finally increased their discharge rate above the ongoing activity measured in still water (Fig. 11 bottom). At a flow speed of 13.5 $cm*s^{-1}$ all but one fiber were flow sensitive (Tab. 1). Sixty-three percent of all fibers did not show a response saturation at the water velocities applied. A linear regression of each data set was computed and revealed that the coefficient of determination (R^2) of 85.7% (n=36) of these fibers was ≥ 0.6. Thus most fibers showed an increase in discharge rate with increasing flow velocities. Note that the slopes of the linear regressions showed a broad distribution (Fig 1 inset).

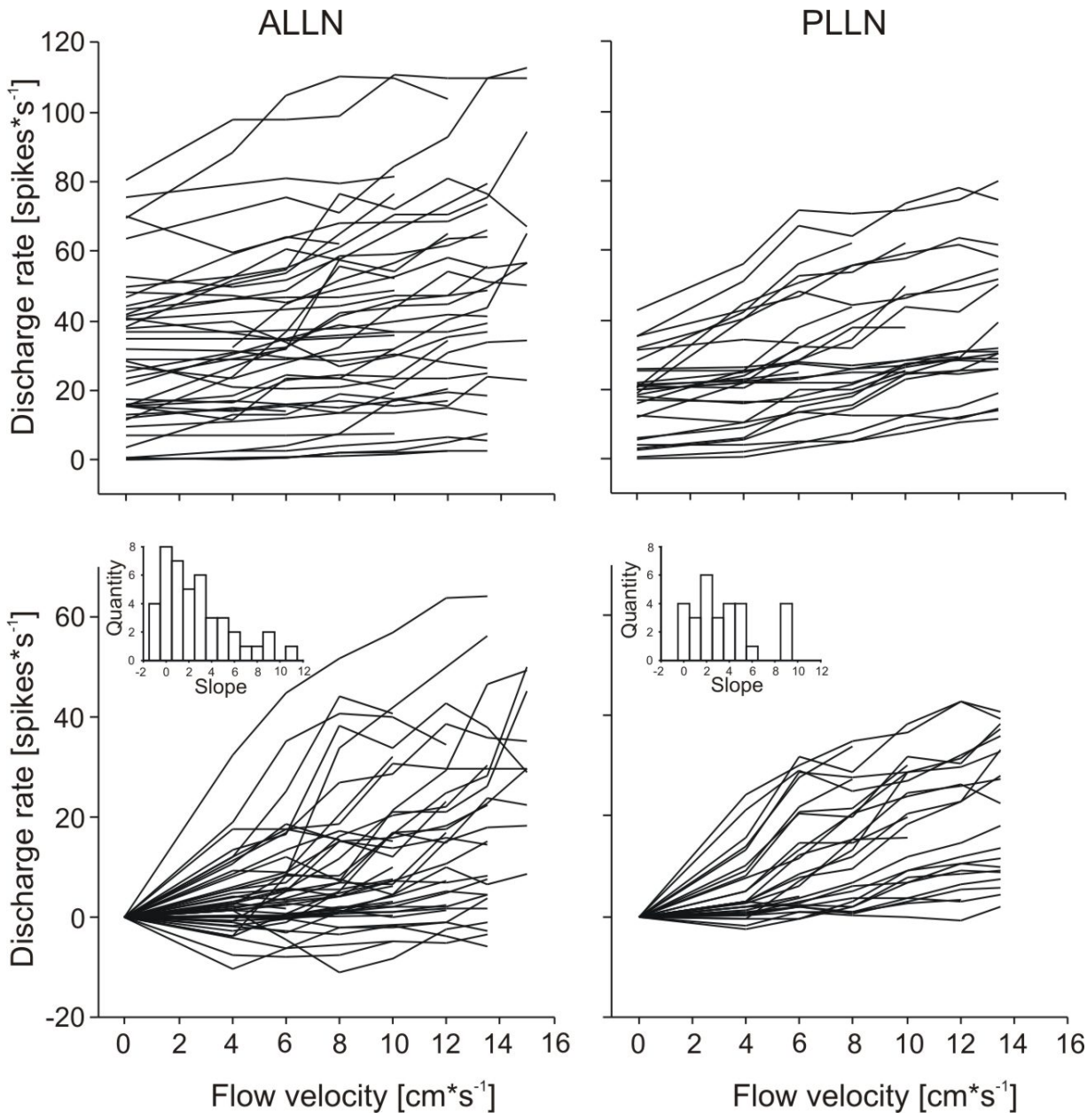

Fig 11: Discharge rates of ALLN fibers (left; n=42) and PLLN fibers (right; n=29) to unidirectional water flow. Top: absolute spike rates. Bottom: absolute spike rates minus spike rate in still water. Note that most units increased their discharge rate with increasing flow velocity. Inset: Distribution of the linear regression slopes.

Flow sensitivity of posterior lateral line nerve fibers

Under still water conditions ongoing activity of PLLN fibers (n = 29) was 19.1 ± 10.8 spikes*s^{-1} (mean ± SD; median: 20.6 spikes*s^{-1}). At a flow velocity of 6.5 cm*s^{-1}, 21 of the 29 PLLN fibers encountered were flow sensitive, i.e. they significantly increased their discharge rates. Eight fibers did not significantly alter their discharge rate at a flow speed of 6.5 cm*s^{-1}. However, with increasing flow velocity more and more of these fibers became flow sensitive (Tab. 2). Three fibers responded with a decrease in ongoing activity at 6.5 cm*s^{-1}. This decrease was, however, not significant. At flow velocities > 6.5 cm*s^{-1} these fibers finally increased their discharge rate above the ongoing activity measured in still water (Fig. 11). At a flow speed of 13.5 cm*s^{-1}, again all but one fiber were flow sensitive (Tab. 2). Eighty-three percent of all fibers did not show response saturation. In 14 PLLN fibers the velocity test was repeated 3 times. In all 14 fibers responses were reproducible from trial to trial (Fig. 12). A linear regression of each data set was computed and revealed that 93.1% (n=27) of the fibers had a coefficient of determination of $R^2 \geq 0.6$. Thus most fibers showed an increase in discharge rate with increasing flow velocities. The slopes of the linear regressions showed a broad distribution (Fig 1 inset).

Table 2. Percentage and number of ALLN and PLLN fibers classified as flow sensitive at different water flow velocities:

Flow velocity [cms^{1}]*	*6.5*	*10*	*13.5*
Flow sensitive ALLN fibers	71 % n = 42	88 % n = 40	96 % n = 27
Flow sensitive PLLN fibers	72 % n = 29	92 % n = 25	95 % n= 20

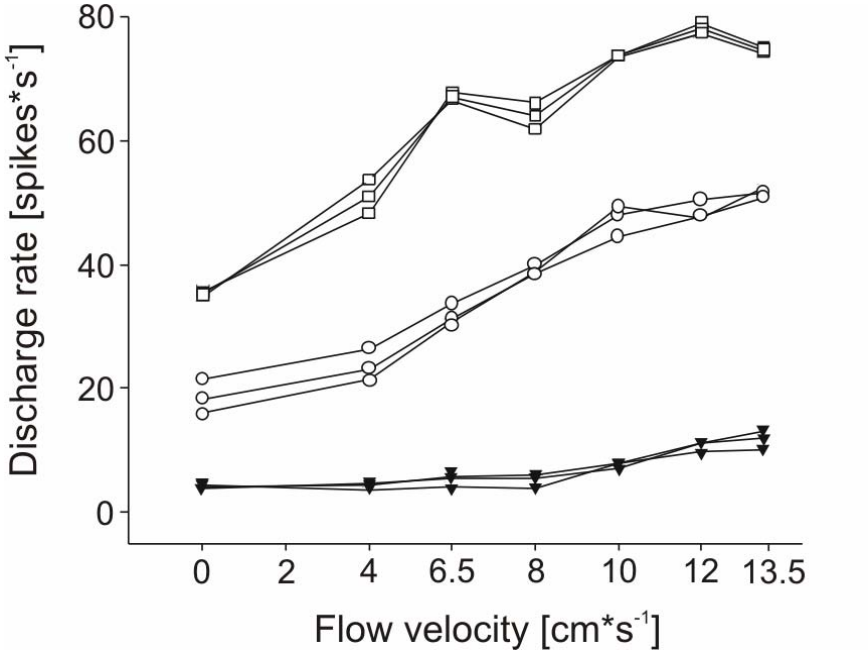

Fig 12: Discharge rates of ALLN fibers as function of flow velocity (different symbols refer to different fibers). Each data point shows the discharge rate averaged over 60 seconds.

Reversal of flow direction

In 12 ALLN fibers it was investigated how flow direction (head-to-tail vs. tail-to-head; flow velocity 10 cm*s^{-1}) affects neuronal activity. Regardless of flow direction all but one ALLN fiber had a higher discharge rate at 10 cm*s^{-1} than at 0 cm*s^{-1}. On average, at a flow velocity of 10 cm*s^{-1} the discharge rates were significantly higher in the head-to-tail (63.94 ± 49.37 spikes*s^{-1}) than in the tail-to-head direction (58.85 ± 48.24 spikes*s^{-1}; paired t-test: n=12, p=0.05).

In 8 ALLN fibers flow velocity response functions (flow velocities 0, 6.5, 10, and 13.5 cm*s^{-1}) were measured (Fig. 13). Irrespective of flow direction (head-to-tail vs. tail-to-head) all but one fiber increased their discharge rates with increasing flow velocity. Fibers showed no significant difference in discharge rates at 6.5 cm*s^{-1} (head-to-tail 50.0 ± 43.1 spikes*s^{-1}; tail-to-head 48.7 ± 43.4 spikes*s^{-1}; paired t-test: n=8, p=0.06). At water flow velocities of 10 and 13.5 cm*s^{-1} the discharge rates of the fibers in the head-to-tail direction were significantly higher than the discharge rates in the tail to head direction (10 cm*s^{-1}: head-to-tail 70.1 ± 54.4 spikes*s^{-1}; tail-

to-head 62.1 ± 52.2 spikes*s^{-1}; paired t-test: n=8, p=0.01 and 13.5 cm*s^{-1}: head-to-tail 83.7 ± 56.9 spikes*s^{-1}; tail-to-head 67.7 ± 54.1spikes*s^{-1}; paired t-test: n=8, p=0.03). Since the responses of ALLN and PLLN fibers revealed no detectable differences toward the unidirectional water flow from (anterior to posterior) it was not attempted to characterize the responses to water flow from both directions in PLLN fibers.

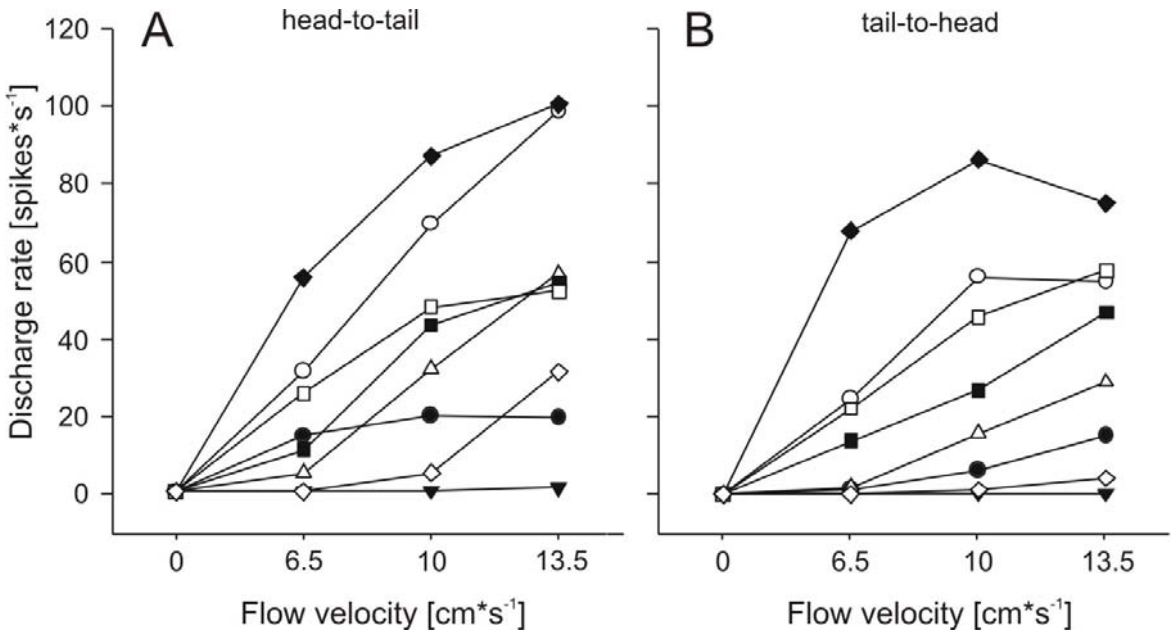

Fig 13: Discharge rate of ALLN fibers (n=8) to water flow from head-to-tail (left) and tail-to-head (right). Each symbol refers to a single unit that was tested in both flow directions. Spike rates obtained in still water were subtracted.

Spike train patterns of LL nerve fibers

In 29 PLLN lateral line nerve fibers the spike train patterns were analyzed. With increasing flow velocity more and more of the flow sensitive fibers showed a burst like activity (for an example see Fig. 14 and Fig. 15). The variability of the instantaneous frequency (IF), displayed for the flow velocities applied, reflects the bursting behavior of these units (for an example see Fig 15, left). The power spectra of the IFs had the largest amplitudes in the frequency range 2 to about 12 Hz. Frequencies in this range correspond well with the burst rhythms of the respective fiber (e.g. Fig. 15, right). Eight units were flow insensitive (water velocity: 6.5 $cm*s^{-1}$). These units barely showed burst like activity, even at high flow velocities (Fig. 16). However, even in units classified as flow insensitive, the variability of the IFs increased (e.g. Fig. 17, left). In addition the power spectrum of the IFs also showed some increase in the frequency range 2 to 10 Hz (Fig. 17, right) if flow velocity was increased.

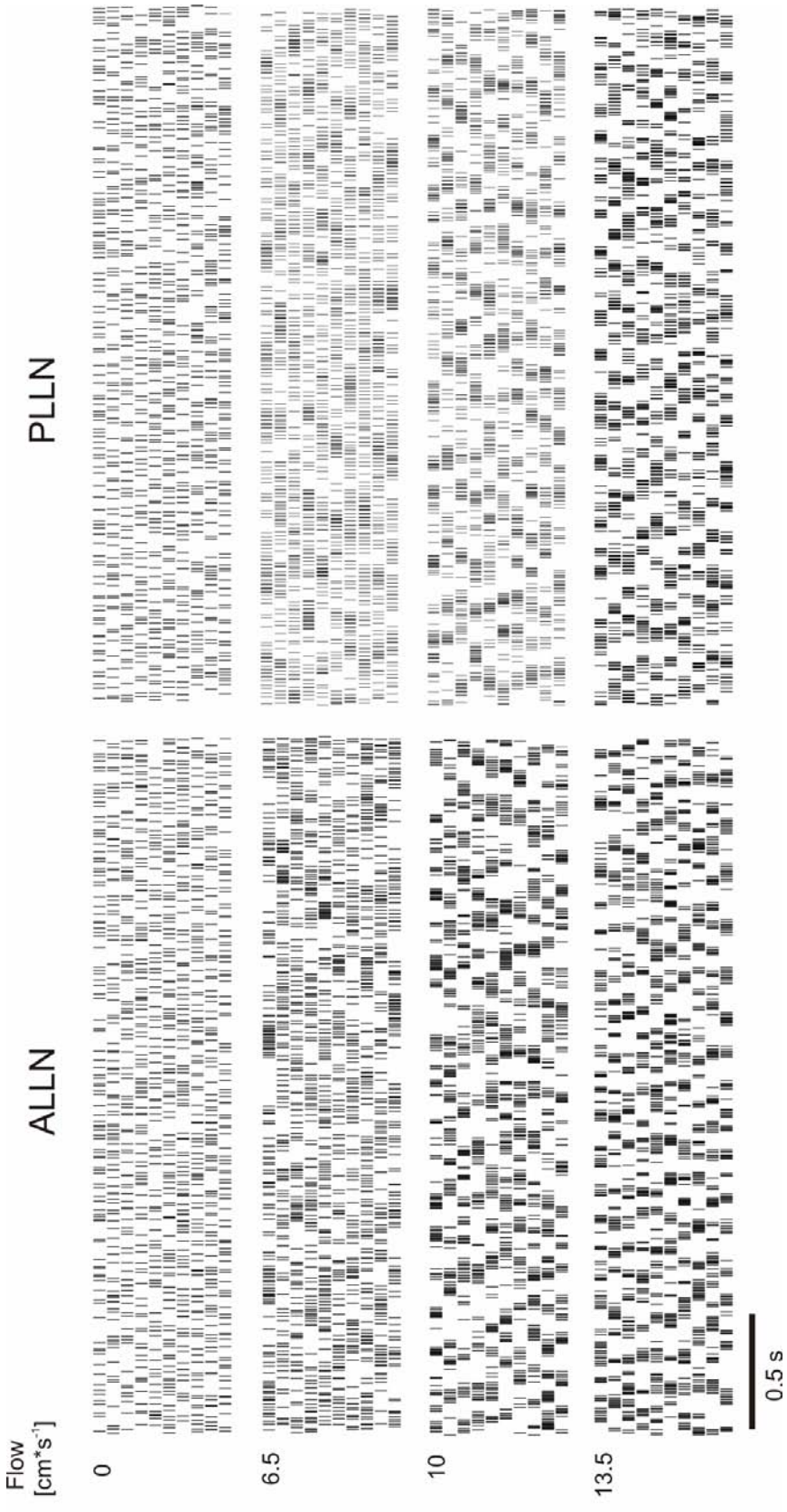

Fig 14: Neural activity of a flow sensitive ALLN fiber (left) and a flow sensitive PLLN fiber (right) exposed to flow velocities of 0, 6.5, 10 and 13.5 $cm*s^{-1}$. Note that higher flow velocities caused burst-like responses.

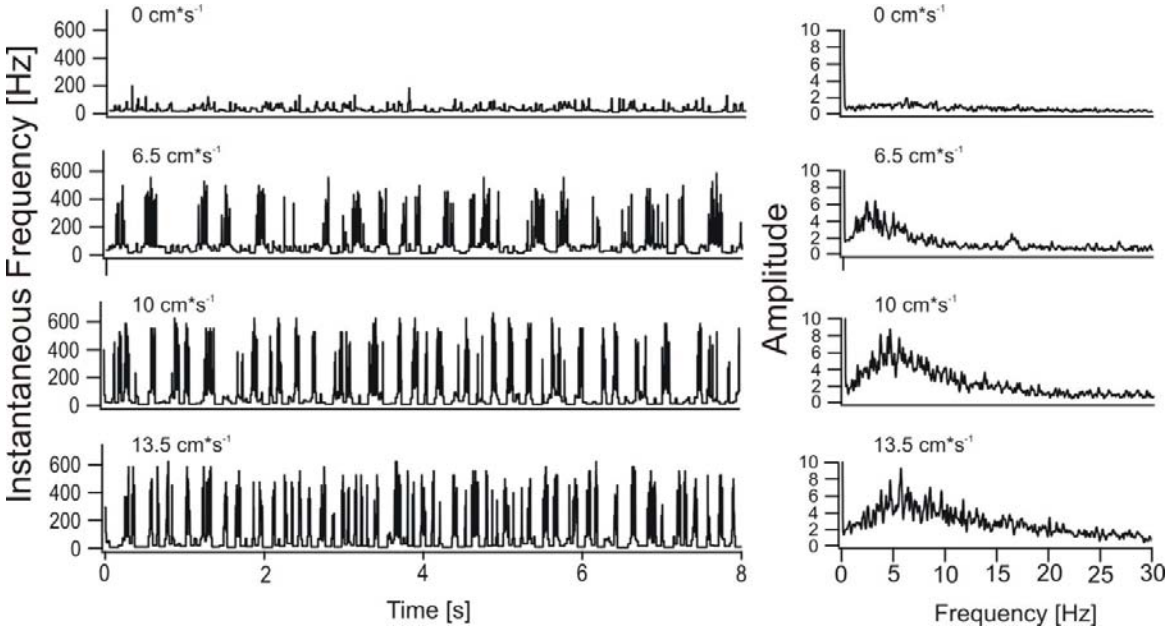

Fig 15: Instantaneous frequency (IF) (left) and corresponding frequency spectra (right) of a flow sensitive PLLN fiber tested at the flow velocities indicated. Burst-like discharges are apparent under flow conditions. The frequency spectra (right) of the IF plots showed a broad peak around 5 Hz. IF and frequency spectra were calculated from the data of the PLLN fiber shown in Fig. 14. For better visualization only 8 s out of 60 s of the IF are shown. Frequency spectra are based on 60 s measurements.

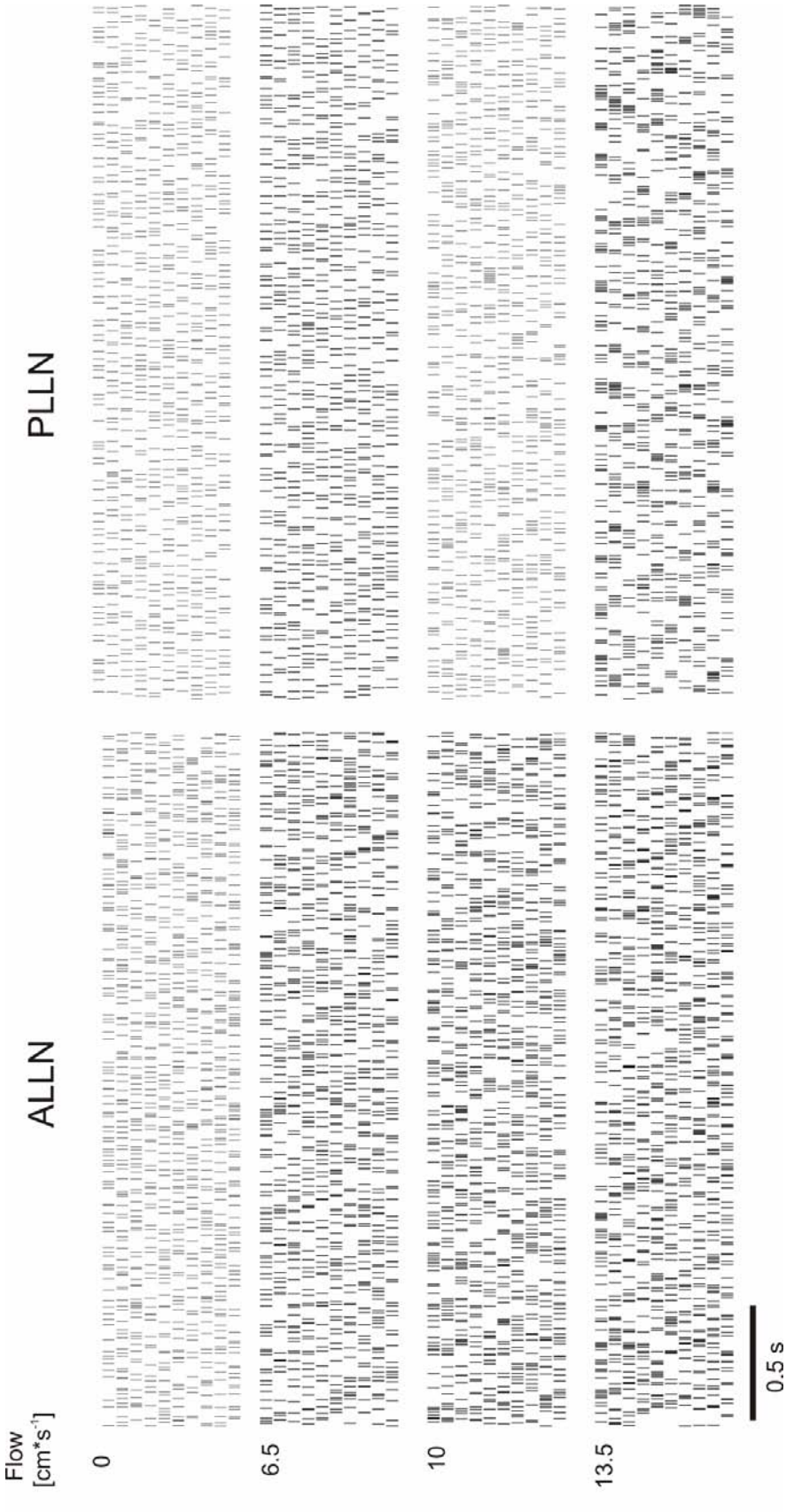

Fig 16: Neural activity of a flow insensitive ALLN fiber (left) and a flow insensitive PLLN fiber (right) tested at the flow velocities indicated.

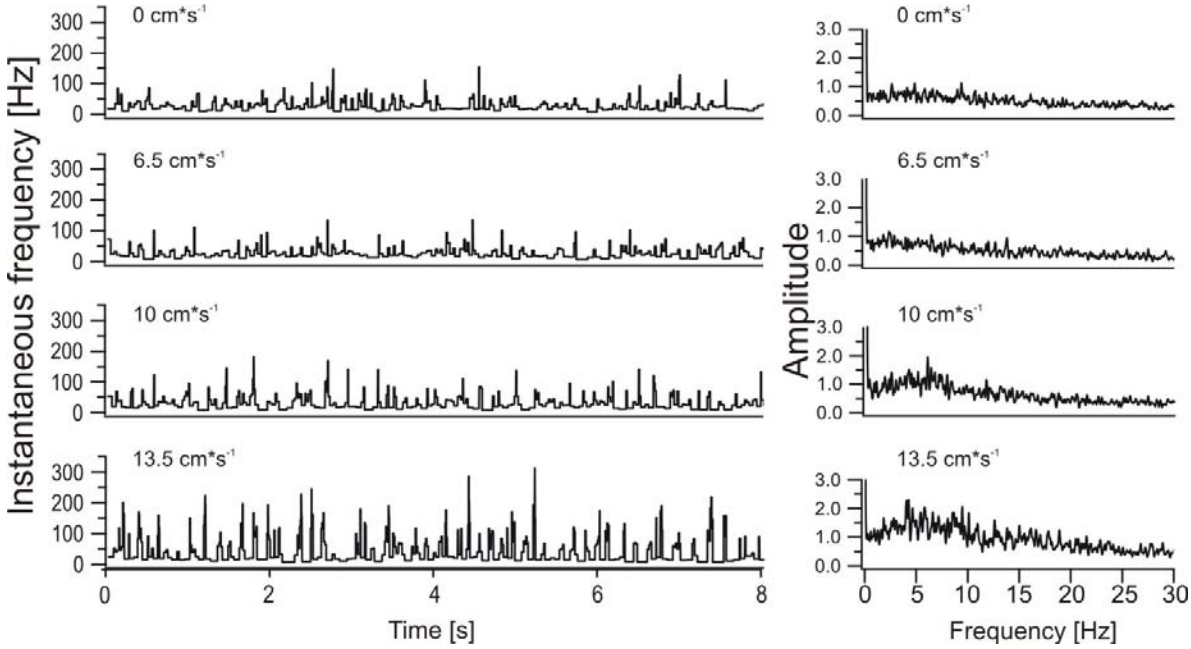

Fig 17: Instantaneous frequency (IF) (left) and corresponding frequency spectra (right) of a flow insensitive PLLN fiber. For better visualization only 8 s out of 60 s of the IF are shown. Frequency spectra are based on 60 s measurements. Data are taken from the PLLN fiber shown in Fig 16.

To quantify the amount of bursting, the RMS (see materials and methods) of the instantaneous frequency (IF) (average rate subtracted) of all PLLN fibers investigated was calculated at the flow velocities 0 to 13.5 cm*s^{-1} (Fig. 18A). The RMS value reflects the normalized variability of the IF. In all units the modulation depth of the spike rate increased with increasing flow velocity. In most cases RMS values > 150% were accompanied by a prominent increase in spike rate (Fig. 18B).

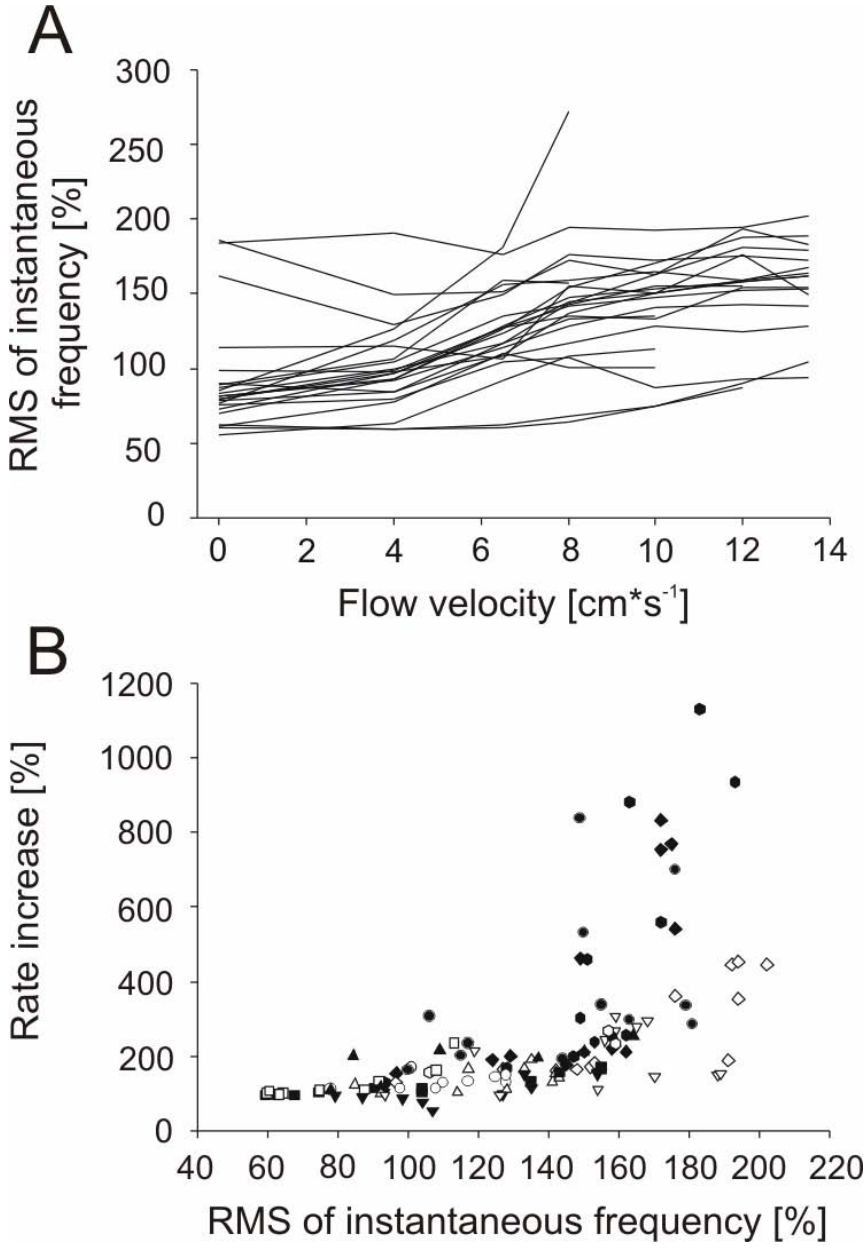

Fig 18 A, B: A: RMS of the IF (average subtracted), expressed in percent of the average spike rate of PLLN fibers (n=25), plotted against flow velocity. B: Normalized RMS values of the IF plotted against the normalized rate increase. Note that in most fibers a rate increase occured only when the RMS values exceeded 150 %.

Flow measurements

To learn to which degree neuronal responses were correlated with hydrodynamic events, water movements were measured with PIV. Flow velocity was retrieved from the PIV data (vector length) at twelve points, separated by 2 mm in the vertical plane. Measurements were done for eight seconds each (for an example see Fig. 19).

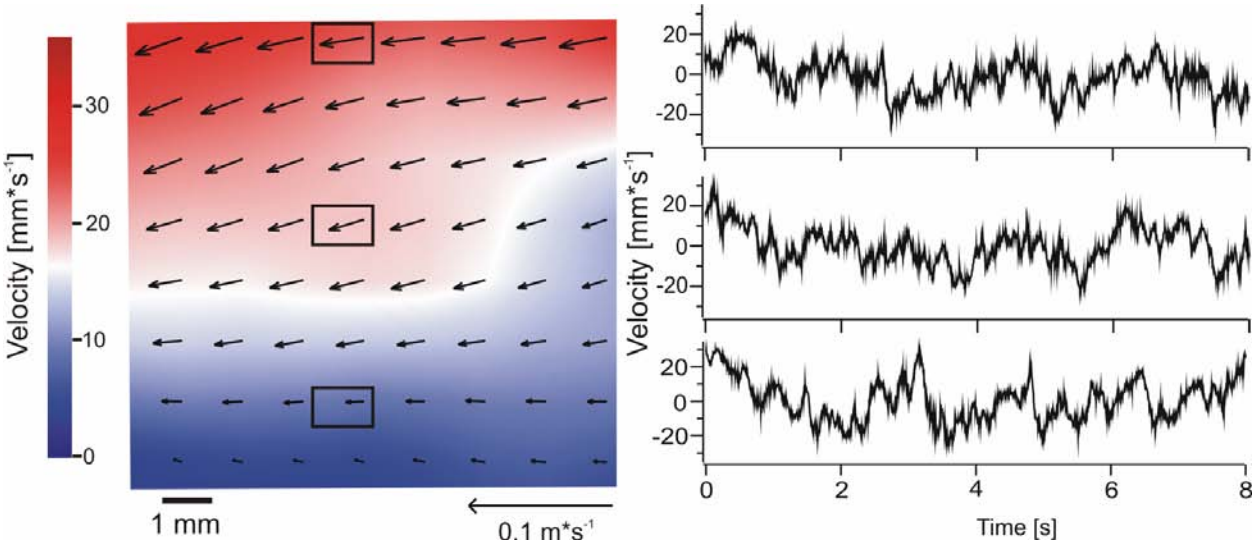

Fig.19: Vector plot (left) and water velocity (right) calculated for a time span of 8 s from the length of the vectors in the interrogation windows indicated by the squares (original PIV plots had a resolution of 32*32 vectors). Background color codes vector length (color code indicated at the left). Black bar indicates spatial resolution, reference vector 0.1 $m*s^{-1}$. Note that from each vector the average vector length (10 $cm*s^{-1}$) was subtracted.

With increasing flow velocity, water movements became increasingly turbulent (Fig. 20, left). At water velocities ≥ 6.5 $cm*s^{-1}$ the spectra showed an increase in power for frequencies < 10 Hz (Fig. 20, right). In contrast to the power spectra of the neuronal data, the spectra of the water motions increased exponentially towards low frequencies (Fig. 20, right). RMS values of the PIV traces (d.c. flow subtracted) showed a linear correlation with water flow velocity (Fig. 21). This finding was independent of flow direction. However, the flow from head-to-tail showed more fluctuations (had larger RMS values) than the flow from tail-to-head (head-to-tail: $0.011 \pm 1.29*10^{-4}$; tail-to-head: $0.006 \pm 1.84*10^{-4}$ (average ±SD); paired t-test: n=12, p≤0.001) (Fig. 22).

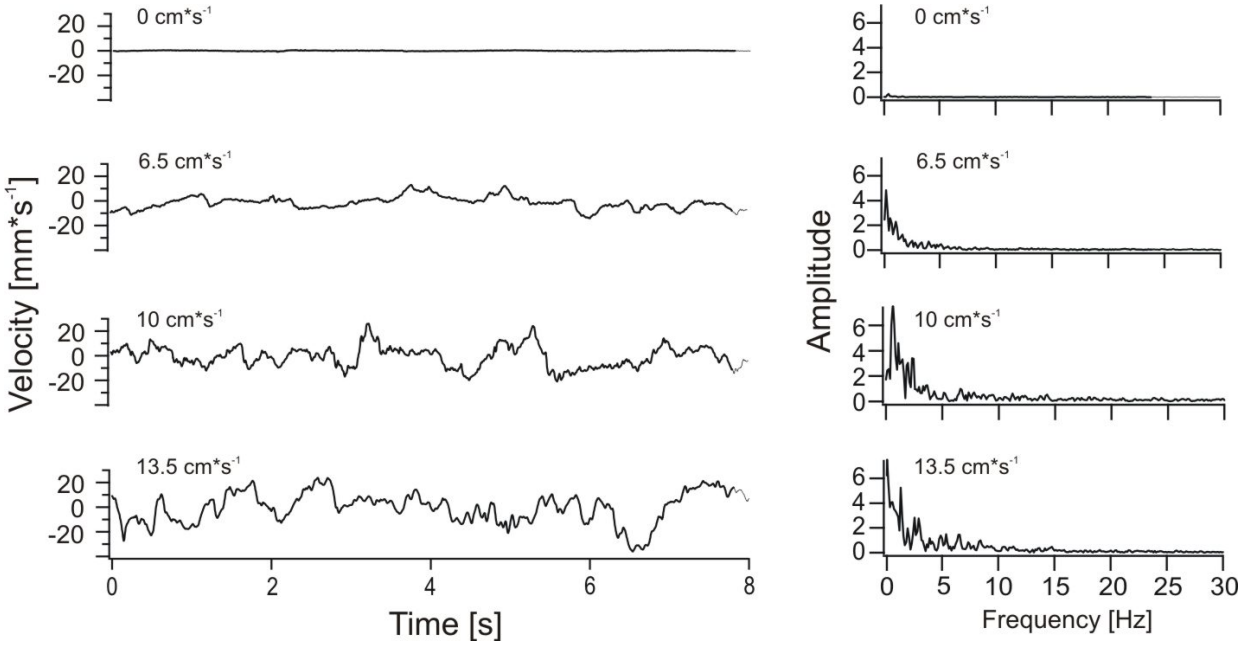

Fig 20: Water velocity as function of time (left) and corresponding frequency spectra (right). Water velocities were retrieved from 4 PIV traces. DC flow velocities were 0, 6.5, 10 and 13,5 $cm*s^{-1}$ indicated. Changes in flow velocity indicate the degree of flow fluctuations. Power spectra are based on 8 s flow measurements. Note that the average vector length (10 $cm*s^{-1}$) was subtracted from each vector.

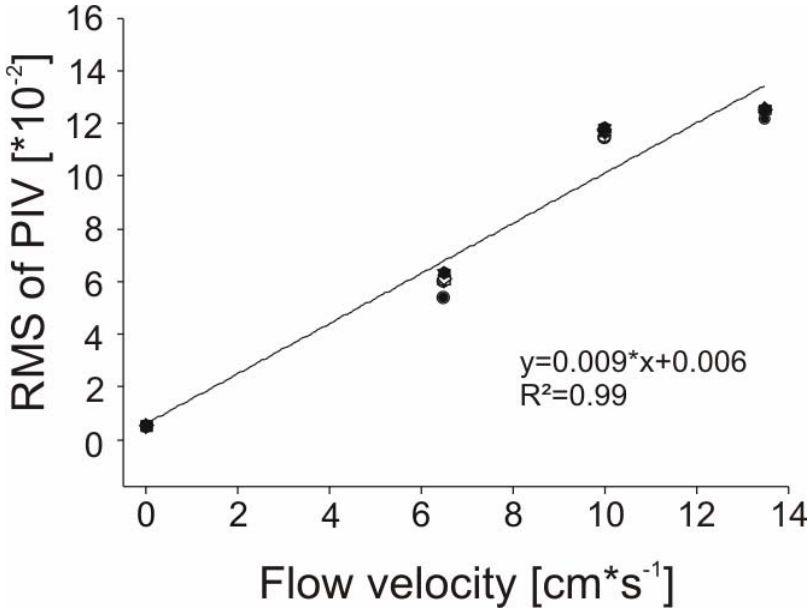

Fig 21: RMS values of PIV traces (n=11) plotted against flow velocity. Line: linear regression of the data. Flow direction was head-to-tail.

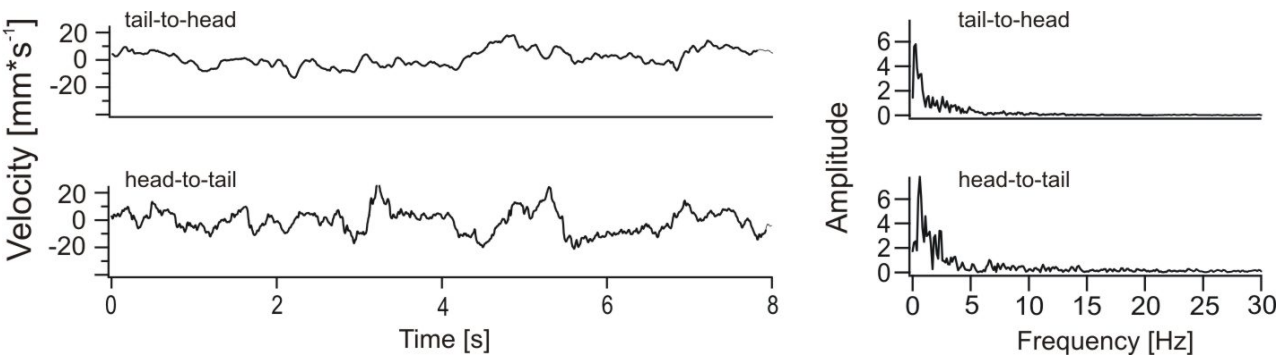

Fig 22: Flow velocity, obtained from PIV data, in the tail-to-head (top) and the head-to-tail (bottom) direction and corresponding frequency spectra (right). Note that average flow velocity (10 cm*s^{-1}) was subtracted.

Spatial analysis of running water

In addition the spatio-temporal flow dynamics was measured with PIV. With increasing flow velocity, the amplitudes of flow fluctuations increased. In addition flow fluctuations showed higher frequencies. The spatial structure of the flow fluctuations was investigated by comparing the fluctuations in an array of 32 x 32 interrogation windows in the PIV plane. For each window (size about 1.5 x 1.5 mm), flow velocity was measured over eight seconds and compared with the flow velocity functions obtained from all other 1023 windows (Fig. 23). A correlation in flow velocity functions occurred only in a small around the reference window. Thus flow fluctuations were spatially non-uniform, as expected from their chaotic nature. However, a comparison of individual flow profiles obtained from interrogation windows arranged in a horizontal and a vertical line (c.f. Fig. 23) showed that the flow fluctuation superimposed on the d.c. flow moved downstream (Fig. 23), i.e. the flow measured in the anterior region of the fish was highly correlated with the flow measured in a more posterior region of the fish (Fig 23), provided the two flow velocity functions were time shifted to compensate for gross flow velocity and for the distance between the two interrogation windows whose vectors were analyzed. Reciprocally the phase shift of the flow velocity functions and the distance between the two interrogation windows can be used to calculate gross flow velocity and flow direction.

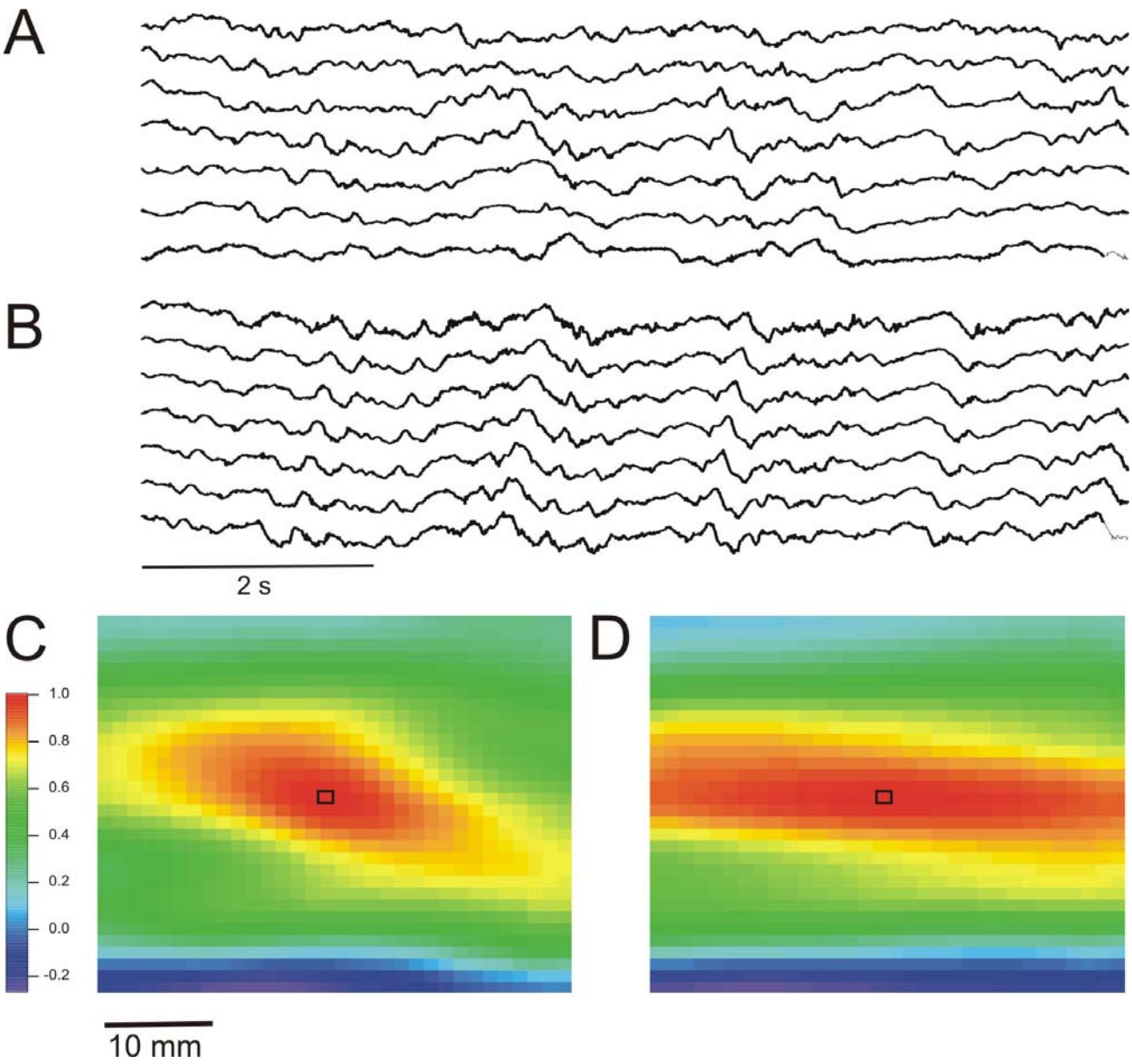

Fig. 23. Flow velocity fluctuations as function of time plotted for the interrogation windows arranged in a vertical (A) and horizontal row (B). Gross flow velocity was 10 cm*s^{-1}. Note that flow fluctuations propagated horizontally in gross flow direction, but not in the vertical direction. C. Color coded correlation of flow velocity functions based on the center vector (reference vector) and all other vectors. Note that the cross correlation (autocorrelation) of the flow velocity functions of the center vector leads to a correlation of 1 (perfect correlation), i.e. to the color red and that with increasing distance from the center (reference) vector the correlation decreased. D. As C but with each flow velocity profile time shifted to correct for flow velocity.

Cross correlation of simultaneously recorded spike trains

To test whether the lateral line system can use flow fluctuations to detect flow direction and flow velocity, pairs of afferent fibers (n=54) were recorded from the PLLN of the goldfish (N = 6). For each pair, neural activities were recorded for 60 seconds. Possible correlations were uncovered by cross-correlating spike train 1 with spike train 2. Since stochastic events like spikes are difficult to correlate, the instantaneous firing frequency (IF) were calculated and used for the cross-correlation procedure.

IF's were cross-correlated for different stimulus conditions. Under still water conditions, ongoing activities of two fibers (42 fiber pairs were tested) recorded simultaneously showed no correlation (-0.1 < correlation factor < 0.3). Under flow conditions most spike train pairs (n=42) also were uncorrelated, however, some pairs (n=12) that did not show a correlation under still water conditions showed a high correlation (0.7 < correlation factor < 1.0) under running water conditions. In general higher flow velocities led to higher correlation coefficients (Fig. 24). As expected the correlation peak shifted with increasing flow velocity in the expected direction (Fig 24).

Correlation peaks could be negative or positive, depending on the position of the neuromast recorded from. As expected, in all fiber pairs that showed a correlation a reversal of flow direction led to a reversal in the sign of the phase shift (Fig 24). One pair showed an almost perfect anti-correlation, i.e. spikes in one fiber never coincided with spikes in the other fiber.

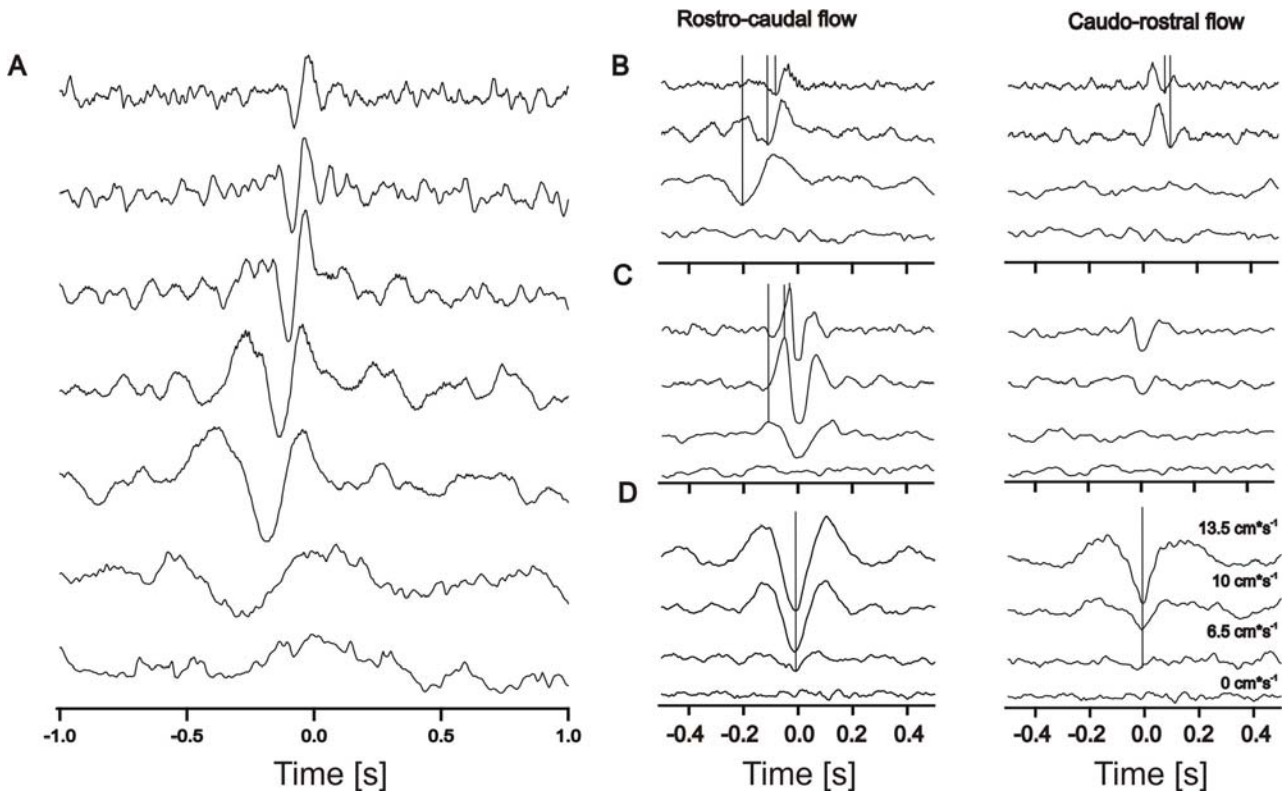

Fig 24. Cross correlation functions of the instantaneous frequency of two neurons recorded simultaneously. A From bottom to top flow velocities were 0, 4, 6.5, 8, 10 and 13.5 $cm*s^{-1}$. Flow direction was from rostral to caudal. B, C, D. Cross correlation functions of the instantaneous frequencies of three neuron pairs recorded simultaneously. Flow was from rostral to caudal (left) and from caudal to rostral (right). Note that the cross correlation functions show correlations (B and C) and anti-correlations (D). Flow velocities were 0, 6.5, 10 and 13.5 $cm*s^{-1}$. It is apparent that higher flow velocities systematically shifted the correlation peaks.

III Responses of lateral line fibers to a Kármán vortex street

Ongoing activity and responses to a Kármán vortex street (KVS)

Single unit recordings were made from 94 fibers in the anterior lateral line nerve (ALLN) of 8 goldfish. Eighty-five fibers responded to water motions (see materials and methods), the remaining 9 fibers did not respond and thus were discarded from further analysis. The ongoing activity of lateral line fibers was determined under still water (SW), running water (RW) and Kármán vortex street (KVS) conditions. Ongoing activity was quantified in terms of spike rate and in terms of the variance of the discharge pattern, expressed by the RMS of the instantaneous frequency. In SW fibers (n = 85) had an ongoing activity of 23.6 ± 19.0 spikes*s^{-1} (median: 20.8 spikes*s^{-1}). In 51 out of the 85 fibers ongoing activity could also be determined under RW conditions (flow velocity: 10 cm*s^{-1}). 45 of the 51 fibers (88 %) significantly increased their discharge rate if exposed to unidirectional water flow (Wilcoxon test, $p \leq 0.01$). These fibers were classified as type I (Engelmann et al., 2002). The remaining 6 fibers (12%) were insensitive to unidirectional water flow (Wilcoxon test, $p > 0.01$). These fibers were classified as type II (Engelmann et al., 2002). Under still water conditions ongoing activity of type I fibers (25.3 ± 18.1 spikes*s^{-1}; median: 22.2 spikes*s^{-1}) was not significantly different from the ongoing activity of type II fibers (35.3 ± 18.5 spikes*s^{-1}; median: 38.5 spikes*s^{-1}; Mann-Whitney U-test: U = 95.0; Z = -1.169; p= 0.25). If exposed to a KVS (n = 46, flow velocity 10 cm*s^{-1}, cylinder diameter 2.5 cm, cylinder position p_0) ongoing activity was 39.6 ± 19.9 spikes*s^{-1}. There was no difference in discharge rate between RW (n = 58; 37.7 ± 21.3 spikes*s^{-1}) and KVS conditions (Mann Whitney U-test: U = 1244.0; Z = -0.589; p= 0.56). The mean RMS value of the instantaneous firing frequency (mean instantaneous frequency subtracted) obtained under RW conditions (65.40 ± 37.70; n = 58) was not significantly different from the mean RMS value obtained under KVS conditions (60.47 ± 36.71; n = 46) (Mann Whitney U-test: U =1276.0; Z =-0.38; p= 0.70).

For further analysis the frequency spectra of the spike trains obtained under SW, RW and KVS conditions were calculated. The frequency spectra of the spike trains showed unpredictable and predictable peaks under both RW and KVS conditions

(Fig 25). Frequency spectra of the spike trains recorded under KVS conditions nearly always (42 out of 46 cases) had one reproducible peak close to the calculated vortex shedding frequency (cVSF) (Fig 25 right). A more detailed analysis of the frequency spectra at the cVSF (0.8 Hz) showed a significant increase in power in the frequency range 0.7 to 1.3 Hz (0.083 ± 0.047 mV; n = 46) only if the fish was exposed to a KVS. If the fish was not exposed to a KVS the corresponding values were 0.066 ± 0.036 mV (RW; n = 58) and 0.033 ± 0.013 mV (SW; n = 85), respectively. Both values were significantly lower than the values obtained under KVS conditions (RW: Mann-Whitney U-test: U = 1036.5; Z = -1.947; p= 0.05; SW: U = 454.0; Z = -7.23; p= 0.001). Due to the small number of type II fibers it was not attempted to statistically analyze the differences between type I and type II fibers.

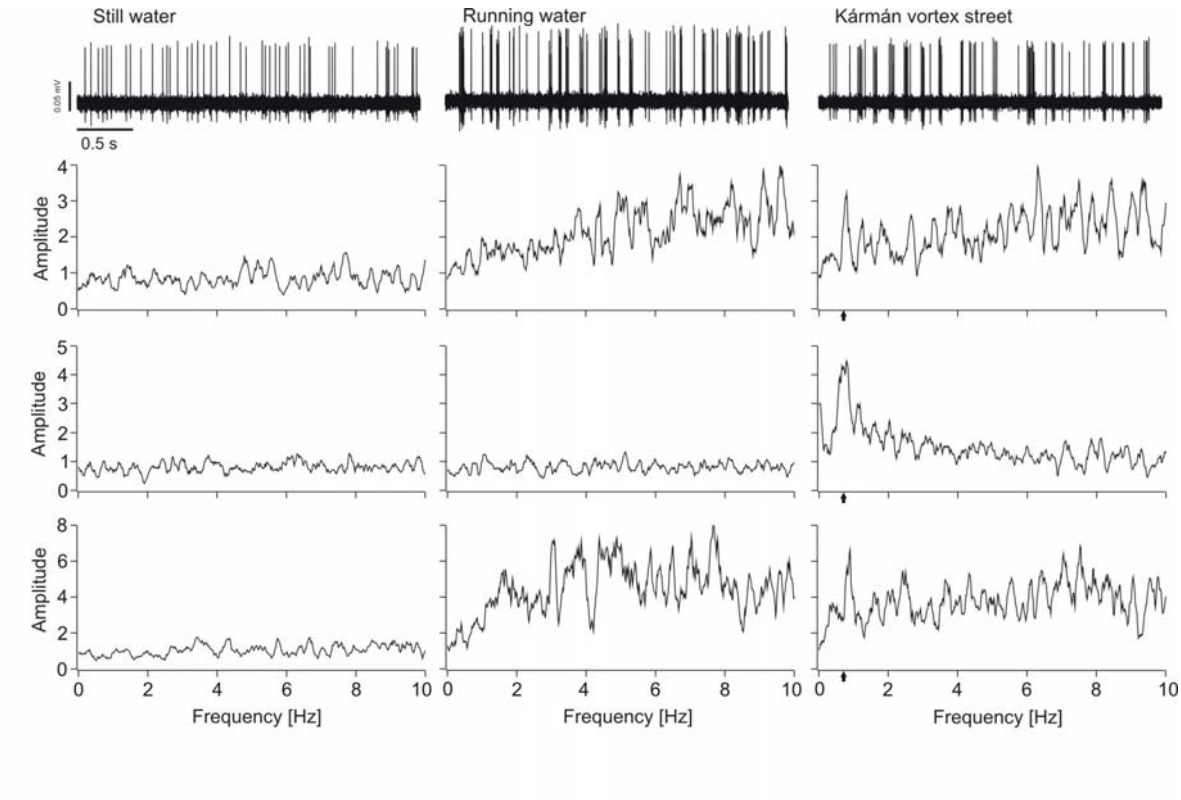

Fig. 25: Frequency spectra of the responses of three afferent fibers (from top to bottom) tested in still water (left), running water (middle, flow velocity 10 cm*s^{-1}), and under KVS conditions (right, cylinder diameter 2.5 cm, flow velocity again 10 cm*s^{-1}). Although most spectra have many peaks, the only peak that was reproducible across fibers was close to the calculated vortex shedding frequency (0.8 Hz, see arrows). The top trace shows the original recording of the primary afferent that provided the data of the top spectra.

Neuronal data and PIV

Flow velocity curves were calculated for each vector of the 1024 (32 x 32) interrogation windows for 2048 successive frames (= 33 seconds) (Fig 26A). For each of the 1024 velocity curves obtained the RMS value was calculated. PIV measurements confirmed (Vogel, 1996) that the water velocity behind a cylinder showed more fluctuations than beneath or in front of the cylinder (Fig 26A). Frequency spectra of the flow velocity curves measured behind the cylinder at positions (40 interrogation windows were analyzed) that were occupied by the fish during the physiological experiments showed a peak close to the cVSF (Fig 26C). This peak was congruent with the first prominent peak in the averaged frequency spectra of the spike trains obtained from recordings done under KVS conditions (Fig 27).

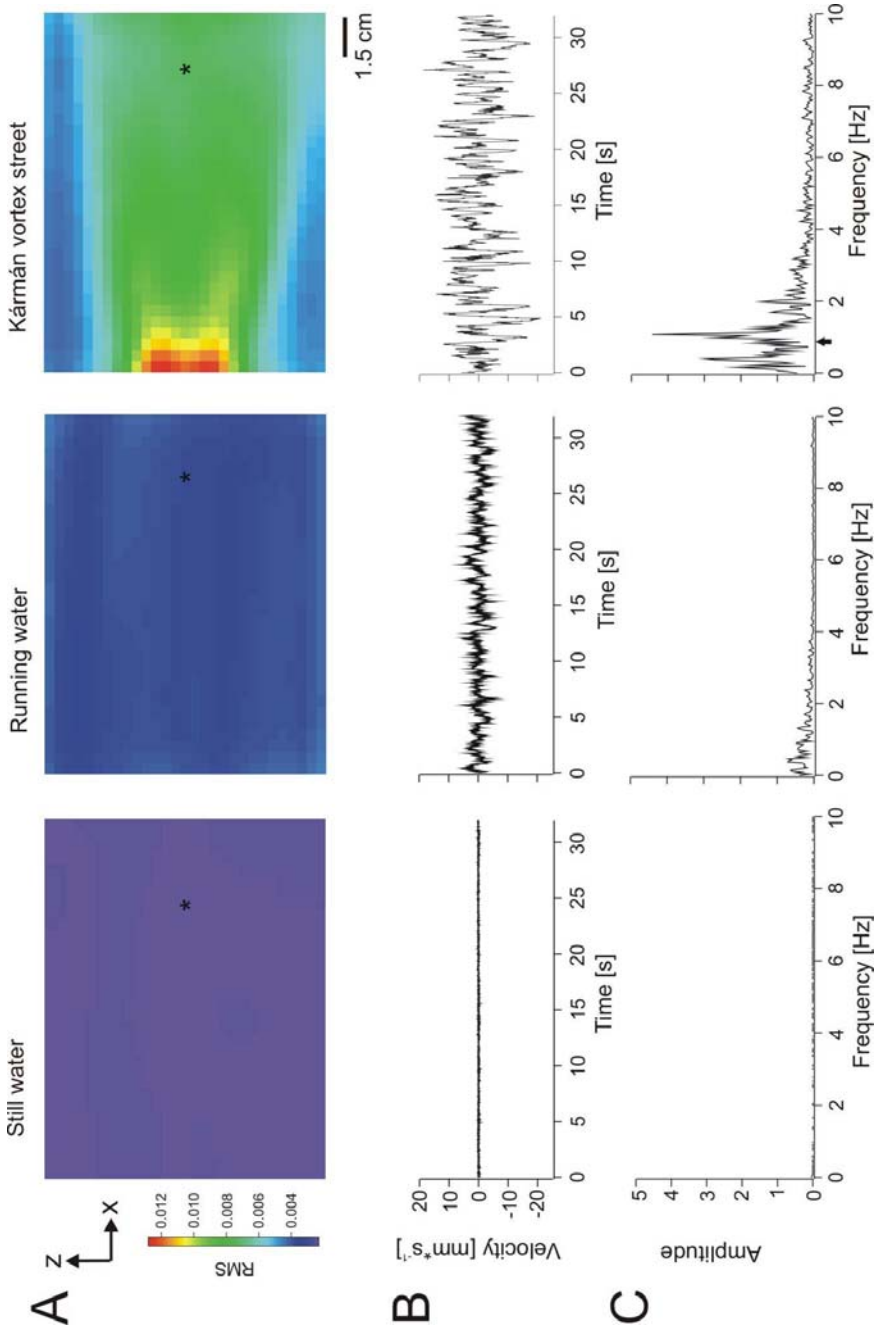

Fig. 26: PIV measurements in still water (left), running water (middle, flow velocity 10 cm*s-1) and under KVS conditions (right, cylinder diameter 2.5 cm, flow velocity 10 cm*s-1). A: Color coded RMS values of flow profiles calculated from a matrix of 32x32 vectors over a time of 33 s. High RMS values in the KVS indicate the presence of flow fluctuations. B: Flow velocity curves calculated for a time span of 33 s from of a single vector. The position of the interrogation window of this vector is marked by an asterisk in A. This was the position of the fish in the physiological experiments, but the PIV measurements shown here were done without a fish. C: Corresponding frequency spectra of the velocity curves shown in B. In the Kármán vortex street large low frequency flow fluctuations are present. The highest peak in the spectrum corresponds to the calculated vortex shedding frequency. Arrow: calculated vortex shedding frequency.

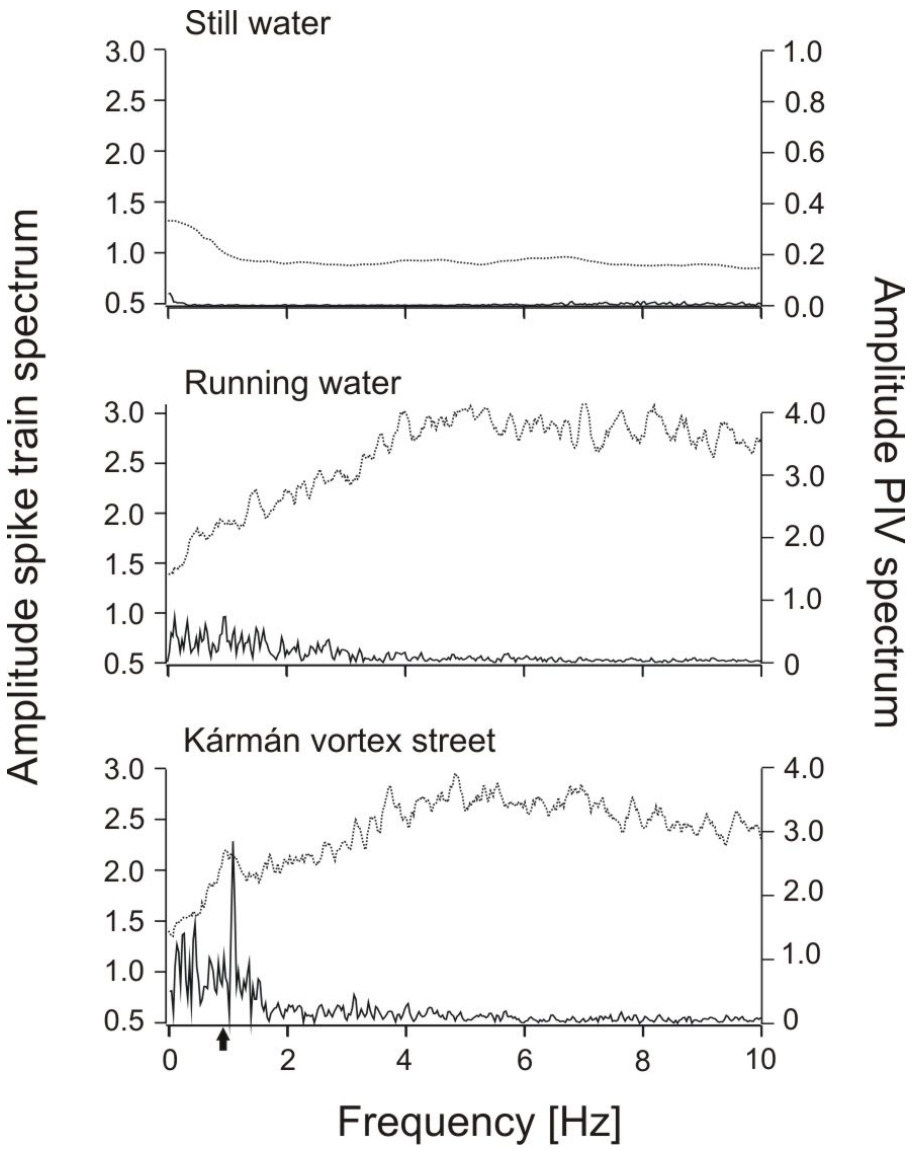

Fig 27: Averaged frequency spectra of the neuronal responses of ALLN fibers (dotted, left y-axis) and of the frequency spectra of corresponding PIV traces (black, right y-axis). From top to bottom: still water, running water (RW, flow velocity 10 cm*s^{-1}) and Kármán vortex street (KVS, cylinder diameter 2.5 cm). Arrow indicates the calculated vortex shedding frequency.

In contrast no prominent peak was found in the frequency spectra of the PIV data obtained under SW and under RW conditions (Fig 27).

Lateral position of the cylinder

Fish (trout) swimming in a KVS continuously change their position (Liao et al., 2003b). In the physiological experiments the position of the fish could not be changed. Instead the position of the cylinder that generated the vortex street was varied. At all cylinder positions (p_0 – p_3, see material and methods and Fig. 1) a prominent peak was found close to the cVSF (cVSF = 0.8 Hz) in the averaged frequency spectra of the spike trains (Fig. 28) (peak positions were: p_0: 1.05 Hz, p_1: 0.86 Hz, p_2: 0.96 Hz and p_3: 1.00 Hz). Regardless of cylinder position the frequency spectra of the PIV data also showed a prominent peak at about 1 Hz (Fig. 27). In the frequency range of 0.7 to 1.3 Hz the position of the cylinder had no effect on the power in the frequency spectra of the fibers (Kruskall-Wallis test: p=0.13) (p_0, n = 46: 0.081 ± 0.046; p_1, n=19: 0.070 ± 0.043; p_2, n=24: 0.090 ± 0.037 and p_3, n=7: 0.109 ± 0.046).

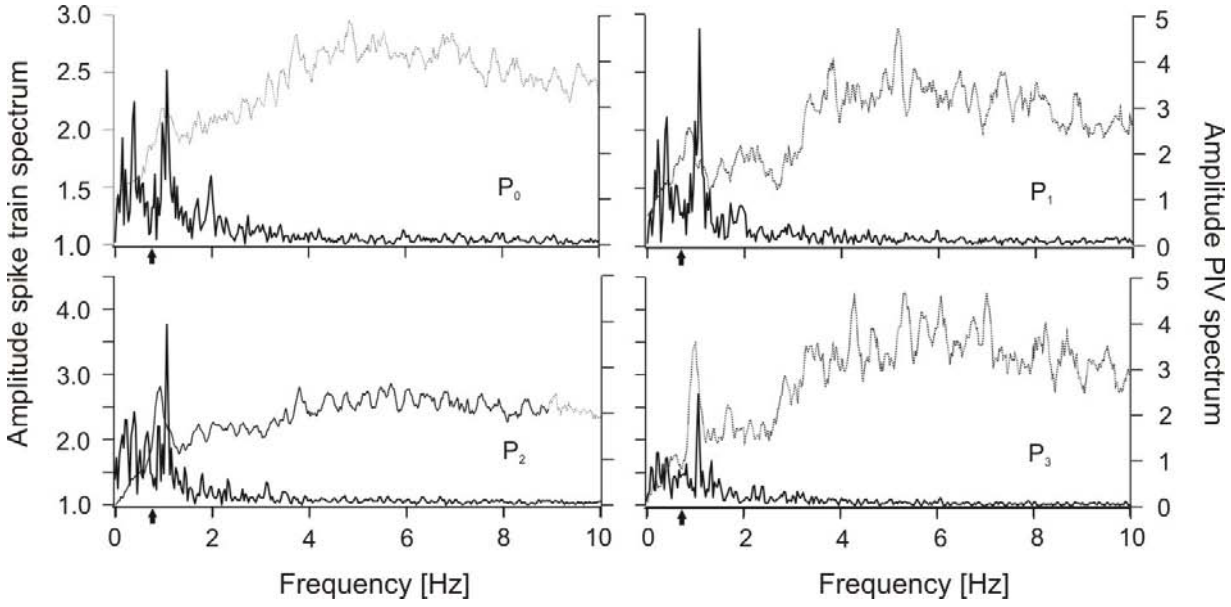

Fig 28: Averaged power spectra of 60 s spike trains recorded from ALLN fibers (dotted line, left y-axis) and of PIV traces (solid line, right y-axis) obtained with the cylinder at the positions p_0, p_1, p_2 and p_3. Arrow indicates the calculated vortex shedding frequency.

Variation of cylinder diameter

As already mentioned the vortex shedding frequency of a KVS depends ot only on water velocity but also on cylinder diameter. Thus any change in cylinder diameter should affect the responses of primary lateral line afferents. The above experiments were repeated with a cylinder that had a diameter of 7.8 cm. This cylinder, placed at the position p_0, also was exposed to a water velocity of 10 cm*s^{-1}. For this condition the cVSF is 0.25 Hz. As expected, the prominent peak in the frequency spectra of the afferent responses now shifted to a lower frequency (0.59 Hz, n = 10). The peak at 0.59 Hz was in agreement with the most pronounced peak in the frequency spectrum of the PIV (0.5 Hz) (Fig. 29). The cVSF of 0.25 Hz is, however, different from both the VSF retrieved from the neuronal and the PIV data.

In a further experiment a cylinder with a diameter of 1 cm was placed at the position p_0 (water velocity again 10 cm*s^{-1}). For this condition the cVSF is 2 Hz. However, in this experiment neither a prominent peak in the spectra of the neuronal data was found nor in the spectra of the PIV data (c.f. Fig. 29).

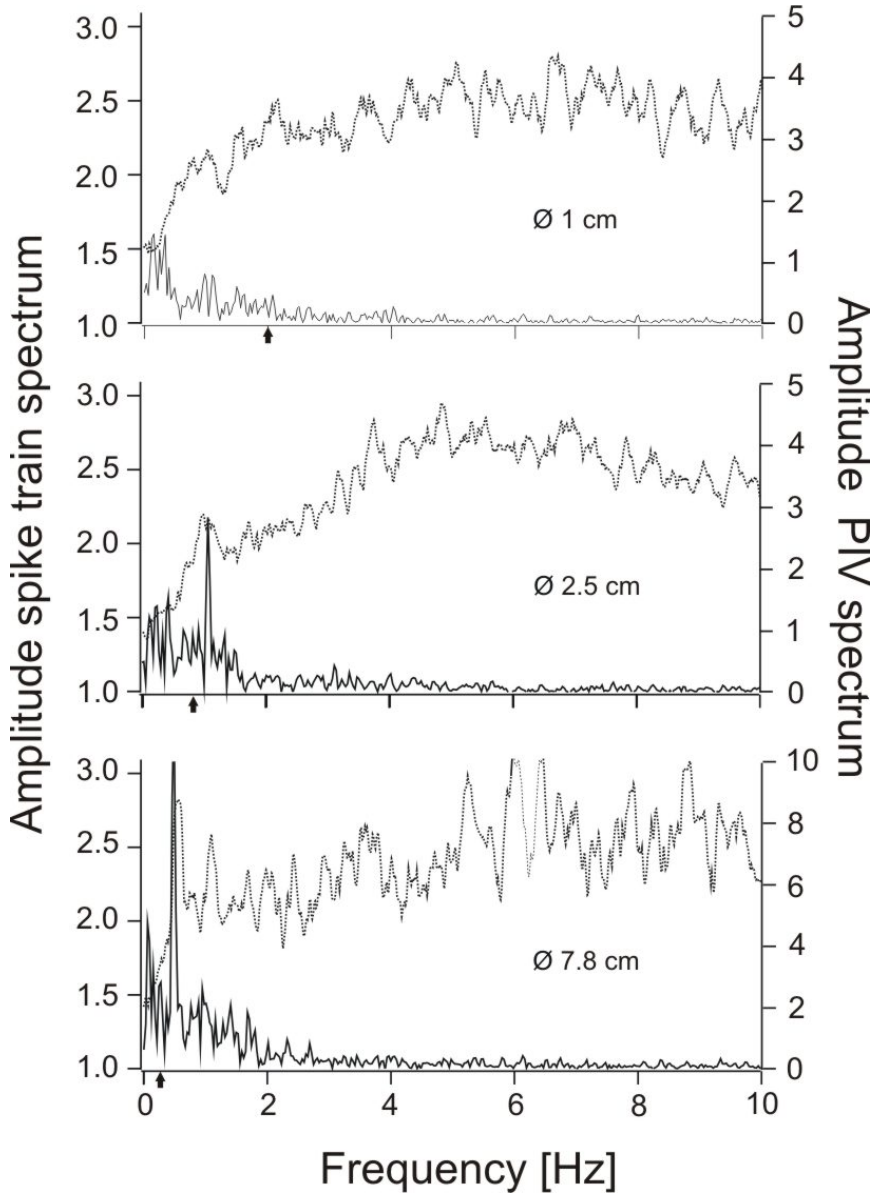

Fig 29: Averaged frequency spectra of the spike trains of ALLN fibers (dotted, left y-axis) and of the corresponding PIV traces (black, right y-axis) under KVS conditions. From top to bottom: cylinder diameter of 1 cm (number of cells: n=32), 2.5 cm (n=46) and 7.8 cm (n=10). Water flow velocity 10 cm*s^{-1}, cylinder position p_0. Arrow indicates the calculated vortex shedding frequency.

Variation of water velocity

The VSF should increase with increasing flow velocity (see formula 1). Therefore the flow velocities 6.5, 10 and 13.5 cm*s^{-1} were applied while using a cylinder with a diameter of 2.5 cm. As expected, the peak in the spectra obtained from the PIV data shifted towards higher frequencies when water velocity was increased (6.5 cm*s^{-1}: 0.6 Hz, cVSF: 0.52 Hz; 10 cm*s^{-1}: 1 Hz, cVSF: 0.8 Hz; 13.5 cm*s^{-1}:1.3 Hz, cVSF: 1.08 Hz). At a flow velocity of 6.5 cm*s^{-1} the spectrum of the neuronal data showed no peak close to the cVSF (0.52 Hz). However, at the flow velocities 10 and 13.5 cm*s^{-1}, the spectra of the neuronal data showed prominent peaks close to the cVSFs (c.f. Fig. 30).

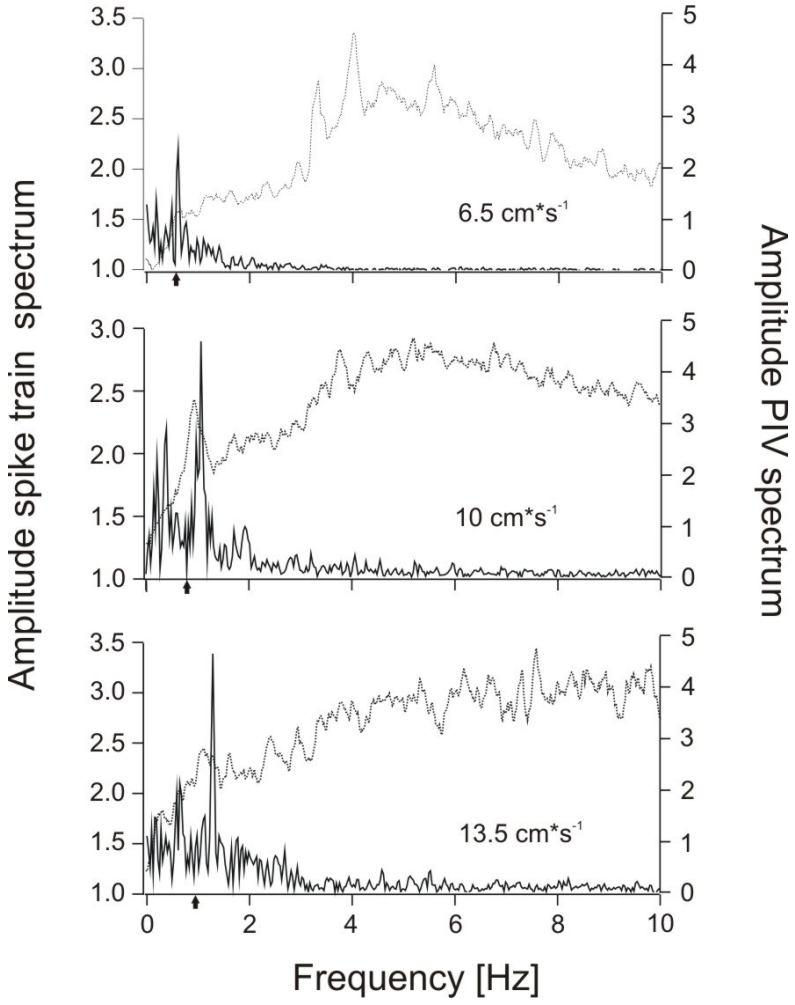

Fig 30: Averaged frequency spectra of the spike trains of ALLN fibers (dotted, left y-axis) and of the corresponding PIV traces (black, right y-axis) under KVS conditions. From top to bottom, water flow velocity was 6.5 (number of cells: n=14), 10 (n=96) and 13.5 cm*s^{-1} (n=24) (cylinder diameter 2.5 cm, Position p_0). Arrow indicates the calculated vortex shedding frequency.

Discussion

I Responses of ALLN fibers to dipole stimuli

It was investigated, how afferent fibres of the ALLN of goldfish respond to running water and to sinusoidal wave stimuli presented in still and running water. In goldfish, the ALLN consists of a dorsal and ventral root that enter the brainstem as one nerve (Puzdrowski, 1989). Recordings were made from both roots but predominantly from the ventral root of the ALLN since it is more accessible in dorso-ventral electrode penetrations. As in previous studies (Engelmann et al., 2002; Engelmann et al., 2000), it was distinguished between type I and type II ALLN fibres based on their sensitivity to a 10 $cm*s^{-1}$ water flow. Flow-sensitive fibres (type I) increased their discharge rates in running water compared to still water rates. The discharge rates of flow-insensitive fibres (type II) in running water were comparable to those in still water. These findings are in agreement with previous studies on PLLN fibres (Engelmann et al., 2002; Engelmann et al., 2000). These studies suggest that type I ALLN fibres most likely innervated superficial neuromast that were permanently stimulated by background water flow resulting in altered discharge rates of the innervating fibres. In contrast type II ALLN fibres most likely innervated canal neuromasts that are not or only weakly stimulated by running water. The ratio between type I and type II fibres in the ALLN (119:34) was comparable to the ratio between type I and type II PLLN fibres in the goldfish (72:28) (Engelmann et al., 2002). Puzdrowski (1989) reported about 1000 superficial and up to 100 canal neuromasts on the goldfish head. Since individual afferent fibres may innervate more than one SN (Münz, 1989), the reported ratio is in fair agreement with the relative proportions of CN and SN.

The ongoing activity of ALLN fibres under still water conditions measured in this study (type I 27.2 ± 25.5 $spikes*s^{-1}$; mean ± SD, type II 26.9 ± 18.7 $spikes*s^{-1}$) are comparable to those reported for goldfish PLLN fibres (Engelmann et al., 2002): type I 30.1± 21.6 $spikes*s^{-1}$, type II 26.1± 23.8 $spikes*s^{-1}$ (Chagnaud et al., 2006): type I 19.3 ± 10.6 $spikes*s^{-1}$, type II 18.7 ± 14.9 $spikes*s^{-1}$). Moreover, in each of these studies ongoing rates of type I fibres were not different from ongoing rates of

type II fibres. Thus, in goldfish, fibres innervating SNs cannot be distinguished from fibres innervating CNs based on their ongoing discharge rates in still water. This is in contrast to Kroese and Schellart (1992) who reported that in rainbow trout ongoing activities were lower in fibres innervating SNs than in fibres innervating CNs.

Ongoing discharge rates of ALLN fibers, measured under different running water conditions, i.e. with or without a cylinder in the flow, were not different. In addition different cylinder positions had no effect on ongoing discharge rates. This is surprising since the PIV measurements showed that both average and RMS flow velocity changed if a cylinder was placed in the flow. In addition flow velocity and flow fluctuations increased if the cylinder was placed more lateral with respect to the location of the fish (see Fig. 9). However, the differences in flow velocity for different cylinder positions were in the order of only a few $cm*s^{-1}$. The differences in average flow velocity without a cylinder and with a cylinder placed at p_0, p_1 and p_2 were 2.3 $cm*s^{-1}$, 1.3 $cm*s^{-1}$, and 0.3 $cm*s^{-1}$, respectively. In addition, different fibres may have a different sensitivity to water flow (Carton and Montgomery, 2002; Voigt et al., 2000) since they innervate neuromasts that can differ in orientation and/or location relative to the direction of the impinging water flow. These factors may have blurred systematic effects of different flow velocities on discharge rates.

In analogy to the data from PLLN fibres (Engelmann et al., 2002; Engelmann et al., 2000), the results reported herein show a clear functional separation between the two fiber populations in the goldfish ALLN. Responses to sinusoidal stimuli of type I fibres, which most likely received input from SN's, were masked by unidirectional water flow (10 $cm*s^{-1}$). In contrast, type II fibres, i.e. fibres that most likely received input from CN's, responded about equally well to a sinusoidal stimulus under still and running water conditions. Thus, type I fibres, i.e. SNs, are impaired in their ability to represent oscillatory water motions in the presence of background flow, whereas type II fibres, i.e. CNs, can represent oscillatory water motions even in the presence of background water flow.

The degree of masking was highly variable across fibres and complete masking of the responses was observed in only a few cases. In addition, the responses of a few fibres classified as type I were not masked in the presence of running water.

One factor that might explain variances in the degree of masking is a misclassification of fibres. In this study and in previous studies (Engelmann et al., 2002; Engelmann et al., 2000), classification as type I or type II was based on whether or not fibres changed discharge rate in response to a 10 cm*s^{-1} water flow. However, both thresholds and slopes of flow-response functions can be highly variable across fibres (Carton and Montgomery, 2002; Voigt et al., 2000). Thus, it is possible that some fibres barely changed their discharge rate in a 10 cm*s^{-1} water flow and therefore, by the criterion applied, may have been misclassified as flow-insensitive, even though these fibres may readily respond to higher water flow velocities. However, the responses to sine wave stimuli of all fibres that were classified as type II in this study were masked neither in terms of discharge rate nor in terms of phase-locking or both.
Another factor that may have led to a misclassification of fibres as being flow-sensitive is the damming pressure that builds up in front of a swimming fish and in front of a stationary fish that faces running water (Dubois et al., 1974; Hassan, 1992). This may cause pressure differences across the fish's head resulting in a stimulation of neuromasts both on the head surface and within head canals. As a consequence, ongoing rates would increase in running water. Nonetheless, it is conceivable that fibres affected by damming pressure may still be capable of encoding sinusoidal stimuli and therefore their responses to dipole stimuli should not be masked or only little affected by a background water flow.

The degree of response masking of type I fibres to a dipole stimulus increased with increasing flow velocity. Thus, the degree of masking depended on the ratio between stimulus (dipole) and background noise (flow). This result is expected since primary lateral line afferents increase their discharge rate both with increasing displacement of a dipole stimulus (Mogdans and Bleckmann, 1999) and with increasing velocity of an external water flow (Carton and Montgomery, 2002; Voigt et al., 2000).
In the present experiments, displacement amplitudes of the vibrating sphere ranged between a few micrometers and 150 µm, corresponding to water velocities between less than 1 cm*s^{-1}and about 11 cm*s^{-1}at the source (sphere), and background flow velocities were 6.5, 10 and 13.5 cm*s^{-1}. Since nearfield flow

around a dipole source is attenuated with a rate of $1/r^3$ (r=radius of the vibrating sphere) (Kalmijn, 1989), the velocity of the dipole-generated water motions at the surface of the fish was always smaller than the background flow velocities. Nevertheless, complete masking was only observed if the lateral line was stimulated with dipole displacements ≤ 250 µm in rather strong background flows (≥ 6.5 $cm*s^{-1}$).

In some type I fibres, responses were masked in terms of phase-locking but not in terms of evoked discharge rate (Fig. 5B). Fibres of this type were generally not very sensitive to dipole stimuli. They responded even in still water with phase-locked discharges but barely with an increase in discharge rate (compare level-response functions in Fig. 5A and B). However, in a few type I fibres responses were neither masked in terms of phase-locking nor in terms of evoked discharge rates even at the strongest background flow velocity applied (Fig. 5C). A possible explanation is that these fibres were misclassified due to damming pressure as discussed above. It is also conceivable that these fibres were particularly sensitive to dipole stimuli and that background flow velocities greater than those used in the experiments were needed to mask their responses to sinusoidal water motions. Finally, in a few fibers the ability to represent the stimulus generated by the vibrating sphere increased at low flow velocities compared to still water conditions. This result may be due to the fact that these fibres increased their ongoing discharge rates in running water. This increase may have resulted in an increase in overall responsiveness causing stronger dipole-evoked responses and better phase-locking.

PIV measurements revealed that the stimulus generated by the vibrating sphere was superimposed on the background water flow. This physical phenomenon can be demonstrated mathematically by vector addition. The fact that complete masking was observed only if the lateral line was stimulated with very small dipole displacements in rather strong background flows raises the question how lateral line neuromast can detect a small stimulus embedded in a strong background noise. The most likely scenario is that lateral line receptors adapt to d.c. (laminar) flow. Hair cells are known to adapt quickly (Eatock, 2000) and it has been shown that the hair cells of the lateral line system of Xenopus adapt to local flow (Görner,

1963). As a consequence the increased neural activity of the innervating afferent fibres should return to pre-flow levels, i.e. to still water levels after a short period of time. If this was the case, then any a.c. stimulus should be detected even in the presence of background flow, i.e. responses to a.c. stimuli should not be masked. However, adaptation to bulk water flow and a consequent unmasking of dipole-evoked responses has not been observed (Carton and Montgomery, 2002; Engelmann et al., 2002; Voigt et al., 2000). Most likely this is due to the fact that the flow in the experimental tank was not laminar but exhibited velocity fluctuations even at the lowest flow velocities applied. These flow fluctuations can be interpreted as an a.c. component superimposed on the d.c. flow. This a.c. component will prevent the discharge rate from returning to pre-flow levels. PIV measurements revealed that with increasing flow velocity the amplitude of the flow fluctuations increased (Fig 21). If the amplitude of the velocity fluctuations in background flow exceed a certain value, fibres will start to show burst-like activity (Engelmann et al., 2002) in response to the flow and therefore may no longer be capable to respond with phase-locked discharges to a sinusoidal dipole stimulus. Thus if the amplitude of the a.c. component exceeds the amplitude of the a vibrating sphere stimulus, masking occurs.

The ability of ALLN fibers to represent a vibrating sphere stimulus in a water flow was not altered, i.e. the degree of masking was not increased, if a cylinder was placed in the flow. Thus, additional fluctuations introduced by an obstacle in the flow did not affect the responses of ALLN fibers. This was again unexpected since the PIV measurements showed that the RMS of the flow increased with a cylinder placed in the flow, thus creating a more noisy environment.
These results indicate that in the range tested the amount of noise (number of fluctuations) was not relevant for masking. Instead the amplitude of the noise (amplitude of the fluctuations) might cause the masking of the dipole signal. Thus the fibers' responses reflect the combination of both the a.c. signals generated by the fluctuations of the flow and the a.c. signal generated by the vibrating sphere.

II Responses of lateral line fibers to running water

In studies in which lateral line neuromasts were stimulated with a local water jet, afferents responded with an increase or decrease in spike rate depending on flow direction (Bauknight et al., 1976; Görner, 1963). This is due to the directional sensitivity of the hair cells. More recent studies investigated the responses of afferent fibers to sustained unidirectional gross water flow. The responses of lateral line neuromasts to water flow was investigated in the Antarctic notothenioid fish *Trematomus* bernacchii (Carton and Montgomery, 2002), the New Zealand long-fin eel *Anguilla dieffenbachia* (Voigt et al., 2000), and in the trout *Onchorynchus mykiss* and the goldfish *Carassius auratus* (Engelmann et al., 2002; Engelmann et al., 2003). In these fish a tonic increase in spike rate was observed in most units if flow velocity was increased. Only occasionally a fiber was found that decreased its discharge rate, and only at low flow velocities. Taking the antagonistic alignment of hair cells in the sensory epithelium of a lateral line neuromast into account (Flock, 1971), on average only 50 % of all afferent fibers should respond with excitation to unidirectional water flow, i.e. there should be an equal number of fibers that decrease their discharge rate. However, in this study and in the studies of Voigt et al. (2000), Carton and Montgomery (2002) and Engelmann et al. (2002) nearly all afferent fibers increased their discharge rate if the fish was exposed to unidirectional water flow. The present study shows that fibers that increased their rate in one flow direction also increased their rate if the flow direction was reversed (Fig. 13). The small, but significant difference in the amount of rate increase between the different flow directions found in this study may be due to the asymmetrical shape of the fish that may have caused differences in the pressure field around the fish depending on whether the head or the tail faced the flow. Anyhow, since all fibers increased their discharge rate regardless of flow direction, they cannot code gross flow direction. But why do primary afferent fibers never decrease their discharge rate?

The frequency spectra of the afferent spike trains showed an increase in power between 5-10 Hz. This decrease correlated with an increase in power in the PIV spectra that occurred in the same frequency band. However, PIV spectra were dominated by frequencies below 4 Hz. Since these frequencies were greatly attenuated in the spike train spectra, it seems likely that the neuromasts are not

sensitive to these very low frequencies. This, and the fact that they did not change their response properties if flow direction was reversed, further suggests that they did not respond to pure d.c. flow. There are several possible explanations for this. i) the cupulae of SNs are situated within the boundary layer that attenuates low-frequency components, ii) additional flow fluctuations may be introduced by the fish's skin and/or iii) due to adaptation the sensitivity of hair cells may decrease in the presence of a d.c. stimulus (as has been shown in auditory hair cells)(Hudspeth et al., 2000). Unfortunately, the actual cupula movements could not be measured during the recordings, thus the nature of the high pass filter remains obscure.

If primary lateral line fibers do not respond to gross water flow it remains to be explained, why most fibers nevertheless increased their mean firing rate with increasing flow velocity. Both, the discharge rate and the RMS of the instantaneous frequency of anterior and posterior lateral line nerve fibers increased with increasing flow velocity (Figs. 15 and 17, left). Fibers that increased their discharge rate with increasing water flow switched from a fairly regular discharge pattern to a burst-like firing pattern. This was also apparent in the spectra of the responses which showed an increase in amplitude at the burst frequencies (4-10 Hz). Average spike rates increased only if the RMS values of the IFs exceeded about 150% of the ongoing activity measured in still water. This shows that minor flow fluctuations in the tank lead only to a modulation of the firing rates that was not accompanied by increasing spike rates. Only at high flow velocities spike rates were significantly higher than spike rates in still water. A similar phenomenon can be observed if the lateral line is stimulated with a vibrating sphere. In this case afferent fibers show a phase locking of spikes at low stimulus amplitudes that is not accompanied by an increase in spike rate (Engelmann et al., 2002; Münz, 1985). A significant increase in spike rate only occurs at higher stimulus amplitudes. It seems likely that the increase in spike rate in running water, found in this study and in the studies of Voigt et al. (2000) and Carton and Montgomery (2002), were caused by flow fluctuations and not by the constant flow.

It has been proposed that flow sensitive fibers innervate SNs and flow insensitive fibers innervate CNs (Engelmann et al., 2002; Engelmann et al., 2000). However, in this study as well as in all other studies flow response functions did not reveal

the presence of two distinct populations of afferent fibers (Carton and Montgomery, 2002; Voigt et al., 2000). Instead fibers showed a continuum of flow sensitivity and even units that did not significantly increase their spike rate at low flow velocities finally did so at higher flow velocities. Whether a fiber is classified as flow sensitive or flow insensitive depends to a large degree on flow speeds applied. It was therefore not attempted to classify between flow sensitive and flow insensitive fibers. The focus of this study was to determine why flow sensitive fibers increase their rate, but not to determine whether they receive their input from superficial or canal neuromasts.

The results do not exclude the possibility that gross flow velocity is encoded by the lateral line. A simple rate code that is a function of flow velocity, however, is unlikely. Although afferent fibers could code flow velocity indirectly by responding to the increasing flow fluctuations, this would not be a reliable method. At a given flow speed, fluctuations are probably very variable and depend - for instance - on the presence or absence of objects upstream. However, it is likely that fish monitor flow fluctuations as they move across their skin. The complex spatio-temporal flow patterns that emerges probably contains information about flow direction and flow velocity. This information may be analyzed centrally by fish.

In this study the responses of lateral line fibers in a stationary still water fish that was exposed to different flow velocities were explored. The hydrodynamic stimuli such a fish experiences is different from a fish that moves through still water. In still water, there may be no flow-associated fluctuations and the lateral line neuromasts could well change their spike rate according to the relative velocity between fish and water thus allowing the fish to determine its swimming speed. In any case, the data suggest that in running water spike trains of flow sensitive lateral line afferents are caused by flow fluctuations and thus cannot code the direction and velocity of constant flow.

The spatio-temporal flow dynamics measured with PIV revealed that flow fluctuations were spatially non-uniform and propagated with the flow. Thus the time a certain velocity fluctuation needs to move from the neuromast first stimulated to the neuromast second stimulated can be used to calculate flow velocity and flow direction.

To test whether the lateral line system uses the fluctuations to detect flow direction and flow velocity pairs of afferent fibers were recorded and cross-correlated. It was not surprising that under still water conditions there was no correlation between the recorded fibers. According to this and previous studies (Chagnaud et al., 2006; Engelmann et al., 2002; Engelmann et al., 2003; Palmer et al., 2005; Topp, 1983; Weeg and Bass, 2002) the discharge rate and the discharge pattern of lateral line fibers varies.

Under running water conditions most fibers showed no correlation. This again has to be expected, as the flow fluctuations moved horizontally over the fish body and correlated mostly in a horizontal direction. Neuromast are widely distributed on the fish body (Puzdrowski, 1989), therefore it is likely that receptors that differ in their vertical position on the fish body show no or at best a weak correlation. Some fibers showed a correlation under running water conditions that increased with flow velocity. This was most likely due to the fact that the amplitude of the fluctuations also increased with flow velocity as shown by PIV measurements. One pair showed an almost perfect anti-correlation, i.e. spikes in one fiber never coincided with spikes in the other fiber. This most likely was a pair of fibers coming from the same neuromast, but from hair cells with opposite orientations.

Double recordings showed that it is possible to extract flow velocity and flow direction from pairs of lateral line fibers. Whether flow fluctuations are used by the lateral line system has to be demonstrated in behavioral studies.

III Responses of lateral line fibers to a Kármán vortex street

The mechanosensory lateral line consists of receptor organs that are situated either on the surface of the skin or in canals. The lateral line responds to the relative movements of water across the fish's body. There are a number of possible sources for these water motions. The fish's own movements cause large water displacements that could give important information about the flow pattern around the fish during swimming (Hanke and Bleckmann, 2004; Hanke et al., 2000). Furthermore, flow patterns produced by swimming can be reflected or altered by nearby objects, i.e. flow pattern can be used to detect these objects as shown for the blind cave fish (Hassan, 1986). Since it is difficult to investigate the information processing of the lateral line system in freely moving fish, the vast majority of studies investigated stationary fish that were subject to water movements caused by external sources. Perhaps the most widely used stimulus was a vibrating sphere. The advantage of a vibrating sphere stimulus is that the water movements are predictable and well defined (Coombs et al., 1988). Frequency, amplitude and phase of the sinusoidal water movements caused by a vibrating sphere are easily controlled. The disadvantage of such a stimulus is that it is only one out of many stimulus types the lateral line system is exposed to under natural conditions. Therefore, a variety of other stimuli were used to study lateral line physiology. The stimuli included moving objects (Engelmann et al., 2003; Mogdans and Bleckmann, 1998) and constant unidirectional water flow (Carton and Montgomery, 2002; Engelmann et al., 2002; Engelmann et al., 2000; Voigt et al., 2000). The disadvantage of these latter stimuli is that they are quite variable and that the exact water flow at any given receptor can neither be controlled nor exactly quantified.

Constant flow caused an increase in neuronal activity around 5-10 Hz that correlated with an increase in flow fluctuations of water movements in the same frequency band. However, it is not clear whether the cupula movements were determined by flow turbulences only or to secondary turbulences in the boundary layer (Engelmann et al., 2002). In other words, it is unclear to what extend the

afferent spike trains reflect true flow fluctuations. To investigate this, we generated vortex streets with predictable vortex shedding frequencies.

Recordings from the ALLN have the advantage that the neuromasts recorded from are in the head region. Thus all neuromasts had approximately the same distance to the vortex shedding cylinder (20 cm, i.e. about 2 body lengths). This distance was chosen since swimming fish (trout) position themselves about 2 body lengths downstream from a cylinder placed in the flow (Liao et al., 2003b). The majority of units were flow sensitive according to the criteria of Engelmann et al. (2002). The ratio between flow-sensitive and flow-insensitive fibers was 7.5:1. This is in the range of a recent study on goldfish (Engelmann et al., 2002). Furthermore, the ongoing activity of ALLN fibers in the experiments is in agreement with the ongoing activity measured in the PLLN of goldfish (Chagnaud et al., 2006; Engelmann et al., 2002).

In running water, spike rates of most units increased. Also Fourier spectra showed an increase in power in the range of 4-10 Hz. If measured in a Kármán vortex street, afferent fibers showed a prominent peak in the Fourier spectra close to the calculated VSF. The presence of vortex motions could also be confirmed by the PIV measurements. Further evidence that the prominent peak in the afferent spike train spectra was caused by the vortices is that variations of the VSF by flow speed or cylinder diameter shifted the peak in the expected direction.

Compared to the most prominent peak in the PIV spectra, the VSF peak in the afferent spike train spectra was relatively small. The spike train spectra were dominated by a general increase in power that must have been due to the flow fluctuations that were present in running water even if no Kármán vortex street was present. Especially frequencies above 2-4 Hz were present in the spike trains whereas the PIV data show most of the power below 2 Hz. It is possible that flow fluctuations close to the fish skin were different from the flow fluctuations in the tank. Another possibility is that neuromasts were especially sensitive to frequencies above 2-4 Hz and that they were less sensitive to the low frequency fluctuations that dominated the PIV data, including the VSF. It should be noted that the VSF is the frequency the vortex motions detach from the cylinder. Even if the VSF does not show up in the single spike train spectra, a fish might well be able to detect the high frequency flow fluctuations in the vortex motions.

The results cannot prove that vortex motions and their shedding frequency are relevant for goldfish. There are certainly other filters in the central nervous system that extract relevant information and eliminate noise (Montgomery and Bodznick, 1994). However, here we show for the first time that spike trains of afferent fibers contain the information about the structure of flow fluctuations including the vortex shedding frequency. Turbulent flow patterns in flowing water or caused by moving objects are highly unpredictable but may contain specific information relevant for the fish. By injecting a specific frequency (the VSF) into the water flow, the spectral composition of flow fluctuations was altered and corresponding changes in afferent fiber activity were found. Whether this lateral line information is used by the fish needs to be determined.

References

Batschelet, E. (1981). The Rayleigh test. Batschelet E (ed) Circular statistics in biology, 1st edn. Academic Press, New York,, 54–58.

Bauknight, R. S., Strelioff, D. and Honrubia, V. (1976). Effective stimulus for the Xenopus laevis lateral-line hair-cell system. *Laryngoscope* **86**, 1836-44.

Blaxter, J. H. S. and Fuiman, L. A. (1990). The role of the sensory systems of herring larvae in evading predatory fishes. *J. mar. biol. Ass. U.K.* **70**, 413–427.

Bleckmann, H. (1993). Role of the lateral line in fish behavior. In *Behaviour of Teleost Fishes*, (ed. P. T.J.). London: Chapmann & Hall.

Bleckmann, H. (1994). Reception of hydrodynamic stimuli in aquatic and semiaquatic animals. Stuttgart, Jena, New York: Gustav Fischer.

Blickhan, R., Krick, C., Breithaupt, T., Zehren, D. and Nachtigall, W. (1992). Generation of a vortex-chain in the wake of a subundulatory swimmer. *Naturwissenschaften* **79**, 220-221.

Campenhausen, C., Riess, I. and Weissert, R. (1981). Detection of stationary objects by the blind Cave Fish Anoptichthys jordani (Characidae). *Journal of Comparative Physiology A: Sensory, Neural, and Behavioral Physiology* **143**, 369-374.

Carton, A. G. and Montgomery, J. C. (2002). Responses of lateral line receptors to water flow in the Antarctic notothenioid, Trematomus bernacchii. *Polar Biology* **25**, 789-793.

Chagnaud, B. P., Bleckmann, H. and Engelmann, J. (2006). Neural responses of goldfish lateral line afferents to vortex motions. *J Exp Biol* **209**, 327-42.

Cheng, J. Y. and Chahine, G. L. (2001). Computational hydrodynamics of animal swimming: boundary element method and three-dimensional vortex wake structure. *Comp Biochem Physiol A Mol Integr Physiol* **131**, 51-60.

Coombs, S., Hastings, M. and Finneran, J. (1996). Modeling and measuring lateral line excitation patterns to changing dipole source locations. *J Comp Physiol A Neuroethol Sens Neural Behav Physiol* **178**, 359-71.

Coombs, S., Janssen, J. and Webb, J. F. (1988). Diversity of lateral line systems: Evolutionary and functional considerations. In *Sensory Biology of Aquatic Animals*, eds. J. Atema R. R. Fay A. N. Popper and W. N. Tavolga), pp. 553–593. New York: Springer-Verlag.

Dehnhardt, G., Mauck, B., Hanke, W. and Bleckmann, H. (2001). Hydrodynamic trail-following in harbor seals (Phoca vitulina). *Science* **293**, 102-4.

Denton, E. and Gray, J. (1988). Mechanical factors in the excitation of the lateral lines of fishes. In *Sensory Biology of Aquatic Animals*, eds. J. Atema R. R. Fay A. N. Popper and W. N.Tavolga), pp. 595–617. New York: Springer-Verlag.

Disler, N. N. (1977). Organy chuvstt sisteny bokovoi linii i ikh znachneie v povedenii ryb. (Lateral line sense organs and theirimportance in fish behavior.). *Izd Akad Nauk SSSR (Translated by Israel Program Sci Transl, 1971, avail. Natl Tech Inf Serv, Springfield, VA, as TT 70–54021*.

Drucker, E. G. and Lauder, G. V. (1999). Locomotor forces on a swimming fish: three-dimensional vortex wake dynamics quantified using digital particle image velocimetry. *J Exp Biol* **202**, 2393-2412.

Dubois, A. B., Cavagna, G. A. and Fox, R. S. (1974). Pressure distribution on the body surface of swimming fish. *J Exp Biol* **60**, 581-591.

Eatock, R. A. (2000). Adaptation in hair cells. *Annu Rev Neurosci* **23**, 285-314.

Engelmann, J., Hanke, W. and Bleckmann, H. (2002). Lateral line reception in still- and running water. *J Comp Physiol A Neuroethol Sens Neural Behav Physiol* **188**, 513-26.

Engelmann, J., Hanke, W., Mogdans, J. and Bleckmann, H. (2000). Hydrodynamic stimuli and the fish lateral line. *Nature* **408**, 51-2.

Engelmann, J., Krother, S., Bleckmann, H. and Mogdans, J. (2003). Effects of running water on lateral line responses to moving objects. *Brain Behav Evol* **61**, 195-212.

Flock, A. (1971). The lateral line organ mechanoreceptors. In *Fish physiology*, vol. 5 eds. W. Hoar and D. Randall), pp. 241–263. New York: Academic Press.

Flock, A. and Wersäll, J. (1962). A study of the orientation of the sensory hairs of the receptor cells in the lateral line organ of fish, with special reference to the function of the receptors. *J Cell Biol* **15**, 19-27.

Goldberg, J. and Brown, P. (1969). Response of binaural neurones of dog superior olivary complex to dichotic stimuli: some physiological implications. *J Neurophysiol* **32**, 613–636.

Görner, P. (1963). Untersuchungen zur Morphologie und Elektrophysiologie des Seitenlinienorgans vom Krallenfrosch (*Xenopus laevis* Daudin). *Z vergl Physiol* **47**, 316-338.

Hanke, W. and Bleckmann, H. (2004). The hydrodynamic trails of Lepomis gibbosus (Centrarchidae), Colomesus psittacus (Tetraodontidae) and Thysochromis ansorgii (Cichlidae) investigated with scanning particle image velocimetry. *J Exp Biol* **207**, 1585-96.

Hanke, W., Brücker, C. and Bleckmann, H. (2000). The ageing of the low-frequency water disturbances caused by swimming goldfish and its possible relevance to prey detection. *J Exp Biol* **203**, 1193-200.

Hassan, E.-S. (1986). On the discrimination of spatial intervals by the blind cave fish (Anoptichthys jordani). In *Journal of Comparative Physiology A: Neuroethology, Sensory, Neural, and Behavioral Physiology*, vol. 159, pp. 701-710.

Hassan, E.-S. (1992). Mathematical description of the stimuli to the lateral line system of fish derived from a three-dimensional flow field analysis. *Biological Cybernetics* **66**, 443-452.

Hudspeth, A. J., Choe, Y., Mehta, A. D. and Martin, P. (2000). Putting ion channels to work: mechanoelectrical transduction, adaptation, and amplification by hair cells. *Proc Natl Acad Sci U S A* **97**, 11765-72.

Jørgensen, J. M. and Flock, A. (1973). The ultrastructure of lateral line sense organs in the adult salamander Ambystoma mexicanum. *J Neurocytol* **2**, 133-42.

Kalmijn, A. (1989). Functional evolution of lateral line and inner ear sensory systems. In *The mechanosensory lateral line. Neurobiology and evolution*, eds. S. Coombs P. Görner and H. Münz), pp. 187–216. Berlin, Heidelberg, New York: Springer.

Kanter, M. J. and Coombs, S. (2003). Rheotaxis and prey detection in uniform currents by Lake Michigan mottled sculpin (Cottus bairdi). *J Exp Biol* **206**, 59-70.

Kroese, A. and van Netten, S. (1989). Sensory transduction in lateral line hair cells. In *The Mechanosensory Lateral Line.Neurobiology and Evolution*, eds. S. Coombs P. Görner and H. Münz). New York: Springer - Verlag.

Kroese, A. B. and Schellart, N. A. (1992). Velocity- and acceleration-sensitive units in the trunk lateral line of the trout. *J Neurophysiol* **68**, 2212-21.

Liao, J. C. (2004). Neuromuscular control of trout swimming in a vortex street: implications for energy economy during the Karman gait. *J Exp Biol* **207**, 3495-506.

Liao, J. C., Beal, D. N., Lauder, G. V. and Triantafyllou, M. S. (2003a). Fish exploiting vortices decrease muscle activity. *Science* **302**, 1566-9.

Liao, J. C., Beal, D. N., Lauder, G. V. and Triantafyllou, M. S. (2003b). The Karman gait: novel body kinematics of rainbow trout swimming in a vortex street. *J Exp Biol* **206**, 1059-73.

Linden, P. F. and Turner, J. S. (2004). 'Optimal' vortex rings and aquatic propulsion mechanisms. *Proc R Soc Lond B Biol Sci* **271**, 647-53.

Mogdans, J. and Bleckmann, H. (1998). Responses of the goldfish trunk lateral line to moving objects. *J Comp Physiol A Neuroethol Sens Neural Behav Physiol* **182**, 659-676.

Mogdans, J. and Bleckmann, H. (1999). Peripheral lateral line responses to amplitude-modulated sinusoidal wave stimuli. *Journal of Comparative Physiology A: Neuroethology, Sensory, Neural, and Behavioral Physiology* **185**, 173-180.

Montgomery, J., Baker, C. F. and Carton, A. G. (1997). The lateral line can mediate rheotaxis in fish. *Nature* **389**, 960 - 963.

Montgomery, J. C. and Bodznick, D. (1994). An adaptive filter that cancels self-induced noise in the electrosensory and lateral line mechanosensory systems of fish. *Neurosci Lett* **174**, 145-8.

Münz, H. (1985). Single unit activity in the peripheral lateral line system of the cichlid fish, Sarotherodon niloticus L. J. *J Comp Physiol A* **157**, 555–568.

Münz, H. (1989). Functional organisation of the lateral line periphery. In *The Mechanosensory Lateral Line. Neurobiology and Evolution*, eds. S. Coombs P. Görner and H. Münz), pp. 17–78. New York: Springer-Verlag.

New, J. G., Alborg Fewkes, L. and Khan, A. N. (2001). Strike feeding behavior in the muskellunge, Esox masquinongy: contributions of the lateral line and visual sensory systems. *J Exp Biol* **204**, 1207-21.

Northcutt, G. (1989). The phylogenetic distribution and innervation of craniate mechanoreceptive lateral lines. In *The mechanosensory lateral line: neurobiology and evolution.*, eds. S. Coombs P. Görner and H. Münz), pp. 17-78: Springer-Verlag.

Palmer, L. M., Deffenbaugh, M. and Mensinger, A. F. (2005). Sensitivity of the anterior lateral line to natural stimuli in the oyster toadfish, Opsanus tau (Linnaeus). *J Exp Biol* **208**, 3441-50.

Palmer, L. M. and Mensinger, A. F. (2004). Effect of the anesthetic tricaine (MS-222) on nerve activity in the anterior lateral line of the oyster toadfish, Opsanus tau. *J Neurophysiol* **92**, 1034-41.

Partridge, B. L. and Pitcher, T. J. (1980). The sensory basis of fish schools: Relative roles of lateral line and vision. *Journal of Comparative Physiology A: Sensory, Neural, and Behavioral Physiology* **135**, 315-325.

Pohlmann, K., Atema, J. and Breithaupt, T. (2004). The importance of the lateral line in nocturnal predation of piscivorous catfish. *J Exp Biol* **207**, 2971-8.

Pohlmann, K., Grasso, F. W. and Breithaupt, T. (2001). Tracking wakes: the nocturnal predatory strategy of piscivorous catfish. *Proc Natl Acad Sci U S A* **98**, 7371-4.

Puzdrowski, R. L. (1989). Peripheral distribution and central projections of the lateral-line nerves in goldfish, Carassius auratus. *Brain Behav Evol* **34**, 110-31.

Satou, M., Takeuchi, H.-A., Nishii, J., Tanabe, M., Kitamura, S., Okumoto, N. and Iwata, M. (1994). Behavioral and electrophysiological evidences that the lateral line is involved in the inter-sexual vibrational communication of the himé salmon (landlocked red salmon, Oncorhynchus nerka). *Journal of Comparative Physiology A: Sensory, Neural, and Behavioral Physiology* **174**, 539-549.

Simmons, A. M., Costa, L. M. and Gerstein, H. B. (2004). Lateral line-mediated rheotactic behavior in tadpoles of the African clawed frog (Xenopus laevis). *J Comp Physiol A Neuroethol Sens Neural Behav Physiol* **190**, 747-58.

Späth, M. and Schweickert, W. (1977). The effect of metacaine (MS-222) on the activity of the efferent and afferent nerves in the teleost lateral-line system. *Naunyn Schmiedebergs Arch Pharmacol* **297**, 9-16.

Sutterlin, A. M. and Waddy, S. (1975). Possible role of the posterior lateral line in obstacle entrainment by brook trout (*Salvelinus fontinalis*). *J Fish Res Bd Can* **32**, 2441-2446.

Topp, G. (1983). Primary lateral line response to water surface waves in the topminnow Aplocheilus lineatus (Pisces, Cyprinodontidae). *Pflugers Arch* **397**, 62-7.

Vogel, S. (1996). Life in moving fluids: Princeton University Press.

Voigt, R., Carton, A. G. and Montgomery, J. C. (2000). Responses of anterior lateral line afferent neurones to water flow. *J Exp Biol* **203**, 2495-502.

Webb, J. F. (1989). Developmental constraints and evolution of the lateral line system in teleost fishes. In *The mechanosensory lateral line. Neurobiology and evolution*, eds. S. Coombs P. Görner and H. Münz), pp. 79–97. Berlin, Heidelberg, New York: Springer.

Weeg, M. S. and Bass, A. H. (2002). Frequency response properties of lateral line superficial neuromasts in a vocal fish, with evidence for acoustic sensitivity. *J Neurophysiol* **88**, 1252-62.

Appendix

Rheinische Friedrich-Wilhelms-Universität Bonn, September 2006
Institut für Zoologie
Poppelsdorfer Schloss
53115 Bonn

Erklärung:

Hiermit erkläre ich an Eides statt, dass ich für meine Promotion keine anderen als die angegebenen Hilfsmittel benutzt habe, und dass die inhaltlich und wörtlich aus anderen Werken entnommenen Stellen und Zitate als solche gekennzeichnet sind.

Boris Chagnaud